摘要

基因药物的一种，小干扰 RNA 电荷密度较低且为刚性骨架，与阳性聚合物、脂质体载体复合能力差，导致其包载率低，限制了其在临床中的应用。在本课题中利用亲水性的 siRNA 和疏水性的脂质分子的特性，设计了两亲性的 siRNA 脂质分子（siRNA-phospholipids）键合物，不仅克服了 siRNA 结构呈刚性的问题，又同时提高了 siRNA 包载率。siRNA 脂质分子（siRNA-phospholipids）键合物的合成是将正义链 siRNA 和反义链 siRNA 分别通过二硫键与脂质分子交联，形成正义链 siRNA-lipid 和反义链 siRNA-lipid，再通过退火反应形成。该 siRNA-phospholipids 键合物不仅能够沉默基因表达，而且可作为包载疏水抗癌药物的纳米颗粒的组分。将 siRNA-phospholipids 键合物与阳离子脂质分子、PLGA 和抗癌药阿霉素（DOX）通过纳米沉淀法制备得到纳米颗粒（siRNA-PCNPs）。该纳米颗粒能够将 siRNA 与疏水抗癌药输递进入肿瘤。人宫颈癌体内荷瘤裸鼠模型实验表明，该给药系统能够有效地抑制肿瘤的生长。上述结果表明，siPlk1-PCNPs 是一种极具潜力的安全、有效的基因和抗癌药物输递体系。

Biomaterials 35 (2014) 6519–6533

Contents lists available at ScienceDirect

Biomaterials

journal homepage: www.elsevier.com/locate/biomaterials

SiRNA-phospholipid conjugates for gene and drug delivery in cancer treatment

Hongmei Liu [a,b], Yan Li [a,b], Anbu Mozhi [c], Liang Zhang [a,b], Yilan Liu [a,b], Xia Xu [a], Jianmin Xing [a], Xingjie Liang [c], Guanghui Ma [a], Jun Yang [a,*], Xin Zhang [a,*]

[a] National Key Laboratory of Biochemical Engineering, Institute of Process Engineering, Chinese Academy of Sciences, Beijing 100190, PR China
[b] University of Chinese Academy of Sciences, Beijing 100049, PR China
[c] CAS Key Laboratory for Biomedical Effects of Nanomaterials and Nanosafety, National Center for Nanoscience and Technology of China, Beijing 100190, PR China

ARTICLE INFO

Article history:
Received 23 February 2014
Accepted 11 April 2014
Available online 5 May 2014

Keywords:
Combined effect
siRNA-phospholipids conjugate
Gene silencing
Loading efficiency

ABSTRACT

Due to low charge density and stiff backbone structure, small interfering RNA (siRNA) has inherently poor binding ability to cationic polymers and lipid carriers, which results in low siRNA loading efficiency and limits siRNA success in clinical application. Here, siRNA-phospholipids conjugates are developed, which integrate the characteristics of the two phospholipids to self-assemble via hydrophilic siRNA and hydrophobic phospholipid tails to overcome the siRNA's stiff backbone structures and enhance the siRNA loading efficiency. In this study, the thiol-modified sense and antisense siRNA are chemically conjugated with phospholipids to form sense and antisense siRNA-phospholipid, and then these sense or antisense siRNA-phospholipids with equal amounts are annealed to generate siRNA-phospholipids. The siRNA-phospholipids can serve dual functions as agents that can silence gene expression and as a component of nanoparticles to embed hydrophobic anticancer drugs to cure tumor. siRNA-phospholipids together with cationic lipids and DSPE-PEG2000 fuse around PLGA to form siRNA-phospholipids enveloped nanoparticles (siRNA-PCNPs), which can deliver siRNAs and hydrophobic anticancer drugs into tumor. In animal models, intravenously injected siRNA-PCNPs embedded DOX (siPlk1-PCNPs/DOX) is highly effective in inhibiting tumor growth. The results indicate that the siRNA-PCNPs can be potentially applied as a safe and efficient gene and anticancer drug delivery carrier.

1. Introduction

Gene silencing via RNA interference (RNAi) has been demonstrated as a great potential therapeutic agent for cancer treatment. The emerging RNAi therapy delivers gene-silencing RNAs to the cytoplasm where they recognize and degrade the complementary target mRNA in a sequence-specific manner at a post-transcriptional level [1,2]. However, safe and efficient transduction of siRNAs to target tissues and cells remains a major challenge for clinical trials. Many kinds of nanosized cationic delivery systems have been developed for siRNAs delivery via electrostatic interaction, such as cationic polymers [3–6], cationic lipids and so on [7,8]. However, due to low charge density and stiff backbone structure, siRNA with 21–23 bp nucleotides has inherently poor binding ability to cationic polymers and lipids carriers [9], which results in low siRNA loading efficiency. In order to achieve high loading efficiency for gene transfection, cationic polymers and lipids must be used in an excess amount, whereas they often exhibit severe cytotoxicity [10]. Herein, designing a successful delivery platform with higher siRNA loading efficiency and less cationic materials is a great challenge in therapeutic gene delivery application.

To address this problem, researchers have studied a variety of RNA-based conjugate micro- and nanostructures, such as multimeric siRNA, siRNA homopolymers and microhydrogels for siRNAs delivery, which are designed by facile chemical conjugation and complementary hybridization [11–13]. These siRNA-based conjugate structures can form stable polyion complex formation, which could increase charge density and overcome stiff backbone structure of siRNA, leading to enhanced siRNA loading efficiency and gene silencing ability with less cationic materials. However, these

* Corresponding authors.
E-mail addresses: jyang2012@home.ipe.ac.cn (J. Yang), xzhang@home.ipe.ac.cn (X. Zhang).

http://dx.doi.org/10.1016/j.biomaterials.2014.04.033
0142-9612/

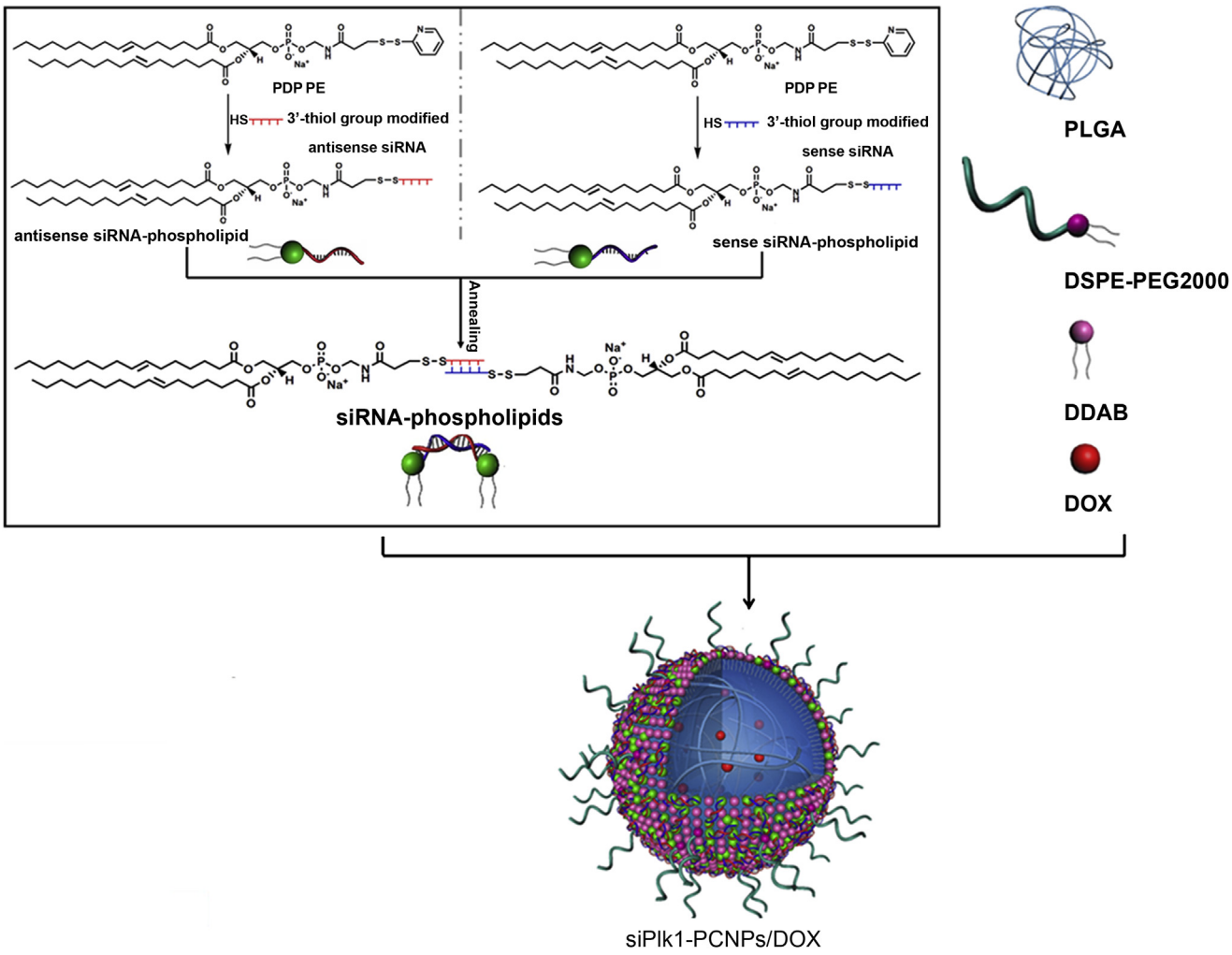

Fig. 1. The synthetic routes of siPlk1-phospholipids and construction of the siPlk1-PCNPs/DOX.

siRNA-based conjugate structures might augment an intracellular immune response, due to remaining as long dsRNA before Dicer-mediated degradation [14]. According to the previous reports siRNA conjugates are desired to disintegrate into monomeric siRNA (mono-siRNAs) in the cell for reduced immune responses [13,15–17]. In order to reduce the immune responses, siRNA-based conjugate should be constructed to have the ability to release monomeric siRNA after internalization into the cells. Therefore, a smart environment-sensitive linkage (a disulfide bond) was employed for programmed release of monomeric siRNA, which can greatly contribute to successful siRNAs delivery.

Herein, we adopted chemically conjugated siRNA-phospholipids as a carrier to change the physicochemical properties of siRNA for overcoming the above-mentioned siRNA delivery difficulties. Since the Polo-like kinase 1 specific siRNA (siPlk1) has greater effect against cancer and has been widely studied according to relevant research literature [18,19]. So, it was used as a model siRNA drug in our work. In this study, the thiol-modified sense and antisense siPlk1 were chemically conjugated with phospholipids to form sense and antisense-phospholipid, and then these sense and antisense-phospholipids with equal amounts were annealed to generate siPlk1-phospholipids. The siPlk1-phospholipids conjugates integrated the characteristics of phospholipids to self-assemble via hydrophilic siPlk1 and hydrophobic phospholipid tails to overcome the siPlk1's stiff backbone structures. These materials could release monomeric siPlk1 under the cytosolic environment. Compared with naked siPlk1, siPlk1-phospholipids conjugates possessed not only negative charges but also amphiphilic structure. Therefore, these chemically conjugated siPlk1 (siPlk1-phospholipids) with two phospholipids fulfill the enhanced loading efficiency of siPlk1 as desired. The siPlk1-phospholipids conjugates, together with Dimethyldioctadecylammonium bromide (DDAB) and 1,2-distearoyl-*sn*-glycero-3-phosphoethanol amine-*N*-methoxy-poly (ethylene glycol 2000) (DSPE-PEG2000), could fuse around ester-terminated poly (D, L-lactic-co-glycolic acid) (PLGA) to form chemically conjugated siPlk1-phospholipids enveloped hybrid nanoparticles (siPlk1-PCNPs) by a single-step nanoprecipitation method [20,21]. We proposed that the siPlk1-PCNPs comprise three layers (Fig. 1): (1) the outer PEG layer, which is expected to prolong the siPlk1-PCNPs circulation time and escape from immunological recognition; (2) the middle layer, which may be composed of siPlk1-phospholipids, cationic lipids (DDAB) and DSPE. It is speculated that small amount of DDAB could be added to balance electrostatic repulsion between negatively charged siPlk1-phospholipids and serve to hold siPlk1s together, thus the siPlk1-phospholipids might form stable and compact structure around PLGA surface; (3) the inner core PLGA polymers, which provide the hydrophobic interaction with siPlk1-phospholipids, DDAB and DSPE-PEG2000 tails, and where encapsulate water insoluble drugs.

Considering the siPlk1-PCNPs' structures, we hypothesized that the siPlk1-PCNPs might exhibit the following advantages: (1) load higher siPlk1 amount with less cationic materials; (2) form stable and compact structure to enhance the colloidal stability in blood environment; (3) release monomeric siPlk1 under a cytosolic environment in the cells; (4) encapsulate hydrophobic drugs (e.g., doxorubicin (DOX)) to kill tumors in combined effects. To test this hypothesis, we developed lipid-PLGA hybrid nanoparticles as control groups, which could electrostatically interact with siPlk1 to form siPlk1-NPs. SiPlk1-NPs and siPlk1-PCNPs have same quality of NPs as well as cationic materials. Compared with siPlk1-NPs, the physicochemical properties, *in vitro* and *in vivo* gene silencing effect of the siPlk1-PCNPs were evaluated. Meanwhile, the combinations of siPlk1 and DOX for tumor treatment *in vitro* and *in vivo* were also investigated.

2. Materials and methods

2.1. Materials

18:1 PDP PE (1,2-dioleoyl-*sn*-glycero-3-phosphoethanolamine-*N*-[3-(2-pyridyldithio) propionate]) was obtained from Avanti. 1,2-distearoyl-*sn*-glycero-3-phosphoethanolamine-*N*-methoxy-poly (ethylene glycol 2000) (DSPE-PEG2000) was purchased from Shanghai Advanced Vehicle Technology Ltd. Co. 4′,6-diamidino-2-phenylindole dihydrochloride (DAPI) and ethidium bromide (EtBr) were purchased from J&K Scientific Ltd. Dimethyldioctadecylammonium bromide (DDAB) and triethylamine (TEA) were bought from Alfa Aesar. DHPE-Texas Red (Texas Red® 1,2-dihexadecanoyl-*sn*-glycero-3-phosphoethanolamine), Lysotracker™ Green and Quant-iT™ RiboGreen® RNA Reagent and Kit were purchased from Invitrogen. Ester-terminated poly (D, L-lactic-co-glycolic acid) (PLGA, MW 38,000–54,000), (3-(4,5-dimethylthiazol-2-yl)-2, 5-diphenyltetrazolium bromide (MTT) and diethylpyrocarbonate (DEPC) were gotten from Sigma–Aldrich. Antibodies against human polo-like kinase 1 (Plk1) and β-actin were obtained from Santa cruz Biotechnology. Goat anti-mouse IgG-HRP antibody, goat anti-rabbit IgG (H + L), BCA Protein Assay Kit, Bradford Protein Assay and lysis buffer (RIPA) were purchased from Beyotime (China). siRNAs targeting human Plk1 (*siPlk1*) (sense strand, 5′-UGAAGAAGAUCACCCUCCUUAdTdT-3′; antisense strand, 5′-UAAGGAGGGUGAUCUUCUUCAdTdT-3′) and scrambled siRNA (*siNonsense*) (sense strand, 5′-UUCUCCGAACGUGUCACGUdTdT-3′; antisense strand, 5′-ACGUGACACGUUCGGAGAAdTdT-3′) were supplied by Su Zhou Ribo Life Science Co. Ltd. (Suzhou, China). In situ cell death detection kit, POD was obtained from Roche (Mannheim, Germany). Tris (2-carboxyethyl) phosphine hydrochloride pierces (TCEP) was purchased from TCI (Japan). Doxorubicin hydrochloride (DOX·HCl) was purchased from Dalian Meilun Biotech Co. Ltd., (Dalian, China) and deprotonated with triethylamine in dimethyl sulphoxide (DMSO) to obtain the hydrophobic DOX. Dulbecco's Modified Eagle Medium (DMEM), penicillin (10,000 U/mL), streptomycin (10 mg/mL), trypsin-EDTA and fetal bovine serum (FBS) were purchased from Thermo.

2.2. Synthesis of siPlk1-phospholipids

The siPlk1-phospholipids were synthesized according to previous report with simple modification [22]. 3′-thiol-modified sense and antisense siPlk1 (sense siPlk1-SH and antisense siPlk1-SH) were treated by TCEP to reduce disulfide protected. In brief, 3% TCEP solution was added to 10 nmol lyophilized thiolated single-stranded siPlk1. After 1 h, 750 μL of absolute ethanol were added to the mixture and vortexed. The mixture solution was centrifuged at 14, 000 g for 20 min. Then, ethanol was decanted and fresh ethanol was added for 3 times to clear residual TCEP. Air dried pellet was dissolved in 10 μL DEPC treated deionized water.

30 nmol of PDP PE dissolved in 10 μL $CHCl_3$ and 100 μL DMSO mixed solution was reacted with sense siPlk1-SH and antisense siPlk1-SH for 24 h at room temperature with gentle stirring to form sense siPlk1-phospholipid and antisense siPlk1-phospholipid. After overnight incubation, the reaction solutions were diluted with 500 μL DEPC treated deionized water and ultracentrifuged three times for 2 min each at 12,000 g using an Amicon Ultra-4 centrifugal filter (MWCO: 10,000, Millipore, Billerica, MA) to remove unreacted PDP PE and produced 2-pyridinethione. SiPlk1-phospholipids were prepared by complementary hybridization between equal amounts of the sense and the antisense siPlk1-phospholipid, which was stirred overnight at room temperature. The siPlk1-phospholipids were characterized by a gel retardation assay for their integrity and saved under −20 °C, and the concentration of siPlk1-phospholipids was determined by measurement of UV absorbance at 260 nm and 280 nm using IMPLEN P330.

The extent of the conjugation of siRNA-phospholipids was analyzed by measuring the released amount of 2-pyridinethione using UV spectroscopy. This method was performed as described previously [23]. In brief, the concentration of 2-pyridinethione was determined by measuring the OD value at 343 nm using TU-1810 ultraviolet and visible spectrophotometer (Beijing, China).

10 μM *N*-succinimidyl-3-(2-pyridyldithiol) propionate (SPDP) was completely reacted with 10 mM DTT for 2 h, which got OD value at 343 nm. This OD value was considered as 100. 30 μM of PDP PE was reacted with 10 μM sense strand siPlk1-SH which measured OD values with different time. The values were represented as the ratio of the OD values of PDP PE reacting with sense siPlk1-SH at different time samples compared to the OD value of SPDP reacting with 10 mM DTT. The percentage of release of 2-pyridinethione was calculated using the following equation:

$$\%\ \text{Release of 2-pyridinethione} = \frac{\text{tV A343}}{\text{sV A343}} \times 100\%$$

sV A343 was the OD values of 2-pyridinethione released from SPDP reacting with 10 mM DTT; tV A343 was the OD values of 2-pyridinethione released from PDP PE reacting with sense siPlk1-SH at different time.

2.3. Preparation of different formation of NPs

SiPlk1-PCNPs were prepared via a single-step nanoprecipitation method [20]. In brief, PLGA and siPlk1-phospholipids were dissolved in DMSO, respectively. DDAB and DSPE-PEG2000 were dissolved in DMSO and $CHCl_3$ mixture (1:1, v/v), respectively. PLGA/DDAB/DSPE-PEG2000/siPlk1-phospholipids (at the mass ratio of 260/30/30/13.3; NPs/siPlk1 weight ratio of 24/1) were added together and vortexed vigorously for 2 min. The resulting mixed solution was slowly dripped into DEPC treated water solution under vigorous stirring conditions for 20 min, and then, followed by gently stirring for 2 h at room temperature. $CHCl_3$ was transferred by vacuum bump. The other remaining organic solvent was separated by using an Amicon Ultra-4 centrifugal filter (MWCO: 10,000 Millipore, Billerica, MA).

The blank NPs were prepared through the same method with PLGA/DDAB/DSPE-PEG2000 (at the mass ratio of 260/30/30). The mixtures were added together and vortexed vigorously for 2 min, and dripped into DEPC treated water solution under vigorous stirring conditions for 20 min followed by gently stirring for 2 h at room temperature. $CHCl_3$ was transferred by vacuum bump. The other remaining organic solvent was separated by using an Amicon Ultra-4 centrifugal filter. The siPlk1-NPs were formed by incubation of blank NPs with siPlk1 at room temperature for 30 min. The complexes were characterized by gel retardation assay for binding of siPlk1 with NPs. The siPlk1-NPs contained PLGA/DDAB/DSPE-PEG2000/siPlk1 at a mass ratio of 260/30/30/4.4 and the NPs/siPlk1 weight ratio of 72/1.

To form siPlk1-PCNPs/DOX and siPlk1-NPs/DOX, DOX was dissolved into the PLGA-DMSO solution, the following operation was similar with the method to prepare the corresponding NPs. The NPs solution was washed three times using a millipore centrifugal filter device (MWCO: 10,000) to remove free DOX. The concentration of DOX in various NPs was measured by UV-Vis analysis. 200 μL of siPlk1-PCNPs/DOX and siPlk1-NPs/DOX solutions were collected separately and mixed with 1800 μL DMSO. The loaded amount of DOX was obtained by quantifying the absorbance of DOX at 485 nm. DOX loading was calculated using the following equation:

$$\text{Drug loading efficiency} = \frac{\text{Amount of DOX in NPs}}{\text{Amount of DOX loaded NPs}} \times 100$$

$$\text{Drug encapsulation efficiency} = \frac{\text{Amount of encapsulation DOX}}{\text{Amount of DOX used for NPs preparation}} \times 100$$

The release of DOX from NPs was examined by incubating NPs in PBS at 37 °C under agitation. PBS was replenished at different time points. Samples were examined by a microplate reader with excitation at 470 nm and emission at 590 nm.

SiPlk1-PCNPs/DiR were prepared just as the method to form siPlk1-PCNPs/DOX. DiR was used instead of DOX.

2.4. Physicochemical characterization

The morphology of the blank NPs, siPlk1-PCNPs and siPlk1-NPs were determined by transmission electron microscopy (H-7650 TEM, Japan). These NPs were dripped on to 200 mesh copper grids coated with carbon and were dyed with 2% phosphotungstic acid. To further ascertain the structure of siPlk1-PCNPs, cryo-transmission electron microscopy (FEI Tecnai 20 Cryo-TEM) was used to take images of NPs in a frozen state.

In order to examine the hybrid NPs structure, fluorescent dye-labeled NPs with micrometer scales were prepared and photographed by using A1Rsi confocal laser scanning microscope (Nikon CLSM, Japan) with a 100 × objective (oil N.A.). Texas Red conjugated lipid (DHPE-Texas Red) and DDAB were dissolved in chloroform and DMSO mixed solution, DSPE-PEG2000 and siPlk1-phospholipids were dissolved in DMSO, and then mixed with DHPE-Texas Red, DDAB, DSPE-PEG2000 and siPlk1-phospholipids. The mixed solution was added dropwise into DEPC treated deionized water and low-speed stirred to self-assemble micrometer particles. Then, the siPlk1-phospholipids were stained using Hoechst 33342. The fluorescence emission of the DHPE-Texas Red (Ex/Em = 595/615 nm) and Hoechst 33342 (Ex/Em = 350/461 nm) was detected by using NIS-Elements Viewer 3.20 confocal operation software.

The hydrodynamic sizes and surface zeta potentials of blank NPs, siPlk1-NPs and siPlk1-PCNPs were measured by a dynamic light scatting (DLS) instrument (Malvern

Nano ZS). Colloidal stability was measured by incubating siPlk1-NPs and siPlk1-PCNPs at concentration of 1 mg/mL in DMEM containing 10% FBS at 37 °C under gentle stirring. At each time point, the mean diameters of hybrid NPs were monitored using DLS.

To evaluate the loading efficiency of siPlk1-PCNPs and siPlk1-NPs with siPlk1, ethidium bromide dye assay was performed as previously described and made some changes [24]. The dye, EtBr, could intercalate between the pairs of siRNA, to form highly fluorescent complexes. SiPlk1-PCNPs and siPlk1-NPs were prepared with the different NPs/siRNA mass ratio of 144/1, 72/1, 24/1 and 12/1. Then, siPlk1-PCNPs and siPlk1-NPs were centrifuged (30 min, 14,000 g, 4 °C) and the supernatant were collected. The supernatant mixed with 12 μg/mL EtBr and detected by fluorescence spectrophotometer (590 nm emission; 490 nm excitation) (Hitachi. Japan). Fluorescence of EtBr in the absence siPlk1 was considered as background and the fluorescence of EtBr-siPlk1 complex with total siPlk1 was considered as 100 and the % relative fluorescence was measured for different samples. The relative fluorescence was calculated using the following equation:

$$\%\ \text{Relative F1.} = \frac{\text{F1. (obs)} - \text{F1. (EtBr)}}{\text{F1. (total siPlk1} + \text{EtBr)} - \text{F1. (EtBr)}} \times 100\%$$

Where Fl. (obs) was the fluorescence of siPlk1-EtBr in supernatant; Fl. (total siPlk1 + EtBr) was the fluorescence of total siPlk1 used binding with NPs; Fl. (EtBr) was the fluorescence of EtBr alone.

To test the loading ability of siPlk1-PCNPs and siPlk1-NPs, the gel electrophoresis was carried out according to the method mentioned above. SiPlk1-PCNPs and siPlk1-NPs complexed with siRNA-phospholipids at NPs/siRNA mass ratio 144/1, 72/1, 24/1 and 12/1, respectively, were prepared for electrophoresis. The gel was visualized by a UV transilluminator at an excitation wavelength of 302 nm.

The siPlk1 loading ratio and encapsulation efficiency were calculated using the following equation:

$$\text{siPlk1 loading efficiency} = \frac{\text{Amount of equivalents siPlk1 in NPs}}{\text{Amount of siPlk1} - \text{phospholipids} + \text{Amount of NPs}} \times 100$$

The weight of NPs was the total weight of DDAB, DSPE-PEG2000 and PLGA.

The amount of siPlk1 released into the supernatant over different incubation time points was measured by Quant-iT™ RiboGreen® RNA Reagent (Invitrogen). SiPlk1-PCNPs were incubated with 10 mM DTT in PBS or in PBS without DTT at 37 °C with gentle stirred. At different time point, the 100 μL samples were obtained and were centrifuged (15 min, 14,000 g, 4 °C) for recovery of the supernatant frozen for storage. For the low-range assay, Quant-iT™ RiboGreen® RNA Reagent 100 μL was added to microplate wells. Samples were excited at 485 and the fluorescence emission intensity was measured at 530 nm, using a fluoreacence microplate reader (SpectraMax M5, Molecular Devices, CA).

The *HeLa* cells were maintained in Dulbecco's Modified Eagle Medium (DMEM) high glucose supplemented with 10% FBS and 1% v/v penicillin/streptomycin at 37 °C with 5% CO_2.

The cytotoxicity of the various NPs was evaluated through the MTT assay against the *HeLa* cells. 4000 cells were seeded on 96-well plates in 100 μL of DMEM medium and incubated at 37 °C in a 5% CO_2 atmosphere for 24 h. The cells were treated with various NPs and incubated for another 72 h. Subsequently, 20 μL MTT was added to each well and incubated for 2 h. Then, the medium was removed and 150 μL of DMSO was added. The absorbance was measured at 492 nm using a plate reader. The percentage of cell viability was determined by comparing cells treated with various NPs with the untreated control cells.

NPs containing both DOX and siPlk1 were prepared as described above. *HeLa* cells (10,000 cells/well) were seeded in 12-well plates and incubated for 24 h at 37 °C in 5% CO_2. Cells were treated with NPs in DMEM containing 10% FBS at 37 °C (5% CO_2) for 120 min. At predetermined time intervals, cells were washed twice with PBS, digested with trypsin solution, and analyzed on a BD Calibur (BD Bio. sciences USA).

To explore the mechanisms underlying the cellular internalization of siPlk1-PCNPs and siPlk1-NPs, the studies of cells uptake were performed at 4 °C or in the presence of chlorpromazine, genistein, mβCD, dynasore and wortmannin [25,26]. Cells were incubated with chlorpromazine (25 μg/mL), genistein (200 μg/mL), mβCD (10 mM), dynasore (80 μM) and wortmannin (100 nM) for 1 h prior to the addition of siPlk1-PCNPs and siPlk1-NPs, which was present in the cell culture medium throughout the uptake experiment for at 37 °C for 2 h. Results were expressed as percentage uptake level of the control cells, which were added siPlk1-PCNPs and siPlk1-NPs without endocytic inhibitors at 37 °C for 2 h.

To determine the localization of NPs, *HeLa* cells (10,000 cells/well) were seeded in a 35 mm glass bottom culture dish and incubated for 24 h at 37 °C in 5% CO_2, allowed to grow until 50% confluent and followed by adding the siPlk1-PCNPs. After 2 h and 8 h of incubation, the cells were washed with PBS twice, and 1 mL of fresh medium containing Lysotracker™ Green (Invitrogen) was added following the manufacturer's instructions. The cells were visualized by CLSM.

HeLa cells were placed on 6-well plates at a density of 50, 000 cells/well and allowed to attach 50% at 37 °C in a 5% CO_2 incubation for 24 h. The *HeLa* cells were transfected with PBS, blank NPs, free siPlk1, nonsense siRNA-PCNPs, siPlk1-PCNPs and siPlk1-NPs for 12 h, and then the culture medium was replaced with fresh DMEM medium. After incubation for another 24 h at 37 °C, the mRNA levels of Plk1 were detected by reverse transcription-polymerase chain reaction (RT-PCR).

RT-PCR was performed as described previously [3]. Primers for Plk1 and GAPDH are as followed: Plk1-forward 5′-AGCCTGAGGCCCGATACTACCTAC-3′, Plk1-reverse 5′-ATTAGGAGTCCCACACAGGGTCTTC-3′, GAPDH-forward 5′-TTCACCACCATGGAGAAGGC-3′, GAPDH-reverse 5′-GGCATGGACTGTGGTCATGA-3′. The mRNA level of Plk1 was normalized to GAPDH.

For Western blot analysis, the cells were lysated with 100 μL of lysis buffer (RIPA) and the supernatant was collected by 4 °C centrifugation for 10 min at 12,000 g. The concentration of protein was measured using the BCA kit. Total 80 μg proteins were loaded on 12% SDS-polyacrylamide gel electrophoresis (SDS-PAGE) and then transferred to acetic nitrocellulose membranes for 90 min (120 V). After sealing with 5% bovine serum albumin (BSA) in PBS with Tween-20 (PBST) for 1 h, the membranes were incubated with monoclonal antibodies against Plk1 overnight. After three times of washing, the membranes were incubated with goat antimouse IgG-HRP antibody for 1 h, and the bands were visualized by DAB staining (0.5 mg/mL with 0.1% H_2O_2).

Terminal deoxynucleotidyl transferase dUTP nick end labeling (TUNEL) assay was used for detecting cell apoptosis and tumor tissues apoptosis. In situ cell death detection kit, POD (Roche) was used to measure apoptosis of *HeLa* cells and tumor tissues, according to the manufacturer's protocol. Briefly, the cells were seeded on slides in 24-well plates for 24 h, and incubated with various NPs in 10% serum conditions for 72 h. The slides were gotten out from 24-well plates, washed with PBS for three times and fixed air dried cell samples with a freshly prepared 4% paraformaldehyde in PBS (pH 7.4) for 1 h at room temperature. Fixed cells were rinsed three times with PBS and incubated with 3% H_2O_2 in methanol for 10 min, rinsed with PBS and immersed in 0.1% Triton X-100 in 0.1% sodium citrate (freshly prepared) for 2 min on ice. The slides were washed three times with PBS, added 50 μL TUNEL reaction mixtures on samples and incubated for 60 min at 37 °C in a humidified atmosphere in the dark. The 50 μL TUNEL reaction mixtures were mixed with 2 μL enzyme solution and 48 μL label solution. After rinsed with PBS for three times, the slides could be analyzed in a drop of PBS under a fluorescence microscope by using 488 nm excitation and 530 nm emission at this state. The cells with green fluorescence were defined as apoptotic cells.

2.5. In vivo experimentation

All protocols for this animal study were conformed the Guide for the Care and Use of Laboratory Animals. All procedures involving experimental animals were performed in accordance with protocols approved by the Committee for Animal Research of Peking University, China. (2×10^6) cells in 100 μL were subcutaneously injected into the armpit of the 5-week-old female BALB/c nude mice. Tumors were allowed to grow to a uniform volume ($\sim 30\ mm^3$).

2.6. Tumor target

siPlk1-PCNPs/DiR (200 μL) were intravenously injected to *HeLa*-bearing mice via tail vein using a syringe. 4 h after injection, the mice were imaged by the Kodak *in vivo* imaging system with excitation at 748 nm and emission at 780 nm.

Free DOX (at 2 mg/kg, 200 μL), siPlk1-NPs/DOX and siPlk1-PCNPs/DOX (at 2 mg/kg, 200 μL) were intravenously injected to *HeLa*-bearing nude mice via tail vein using a syringe. 4 h after injection, the mice were sacrificed and the tumor tissues were harvested. To determine the tumor tissue distributions of siPlk1-NPs/DOX and siPlk1-PCNPs/DOX, DOX fluorescence in the tumor was imaged by the Kodak *in vivo* imaging system with excitation at 470 nm and emission at 600 nm.

Then, the tumor tissues were cross-sectioned using a vibration microtome. In order to stain cell nucleus, the sectioned tissues were incubated in DAPI (0.05 μg/μL) solution in saline for 0.5 h at room temperature. Confocal imaging of tumor tissues was performed using CLSM equipped with 40 × oil objective and filter sets (DAPI (Ex341/Em461), DOX (Ex543/Em570-620)).

2.7. Tissue distribution

Free DOX (at 4 mg/kg, 200 μL), siPlk1-NPs/DOX and siPlk1-PCNPs/DOX (at 4 mg/kg, 200 μL) were intravenously injected to ICR mice via tail vein using a syringe. 1 day after injection, the mice were sacrificed and the tissues were harvested. To determine the tissue distributions of siPlk1-NPs/DOX and siPlk1-PCNPs/DOX, DOX fluorescence in the specimen was imaged by the Kodak *in vivo* imaging system with excitation at 470 nm and emission at 600 nm. Quantitative analysis for the tissue distribution of micelles was carried out using the Living Imaging Software.

2.8. Blood pharmacokinetics

To determine pharmacokinetics, either DOX·HCl (at 4 mg/kg, 200 μL), siPlk1-NPs/DOX or siPlk1-PCNPs/DOX (at 4 mg/kg, 200 μL) was intravenously injected into ICR mice through the tail vein using a syringe [27]. A blood sample (20 μL) was collected from the tail vein at different time points post-injection and mixed with K3-EDTA (0.5 μL, an anticoagulation agent). To extract DOX, acetone (60 μL) was added to the blood, vortexed, and then the solution was centrifuged (5000 g, 10 min). The supernatant was collected and stored at −80 °C until the time of

analysis. The solution was loaded onto 96-well plate in triplicate (50 μL per well). Fluorescence was measured using a microplate reader (SpectraMax M5, Molecular Devices, CA) with excitation at 470 nm and emission at 590 nm. A linear standard curve of DOX ranging 10 ~ 0.1 μg/mL was created and used for measuring the concentration of DOX in blood. The dataset was analysized by PKSlover software. The data of free DOX fit to a one-compartment and the data of siPlk1-PCNPs/DOX and siPlk1-NPs/DOX fit noncompartment pharmacokinetic model. All data were expressed as mean ± SD. $n = 4$.

2.9. Anticancer effect

Anticancer effect of DOX was evaluated by measuring the tumor volume in a double- blinded manner. After reaching a tumor volume by ~30 mm^3, the tumor *HeLa*-bearig mice were randomized into seven groups. The mice received PBS (200 μL), free DOX, free siPlk1 + free DOX, nonsense siRNA-PCNPs/DOX, siPlk1-NPs/DOX, siPlk1-PCNPs/DOX (at 2 mg/kg DOX, 200 μL) and free siPlk1 (1 mg/kg 200 μL), through tail vein injection at day 0, 2, 4 and 6 post initial treatment. Tumor volume was measured as follows:

$$V = \left(a \times b^2\right)/2$$

where a and b represent the major and minor axes of a tumor, respectively. The lengths of the axes were measured using a caliper. Tumor volume in each group was compared by relative tumor volume [28]:

Relative tumor volume = tumor volume/initial tumor volume before treatment

2.10. Measurements of Plk1 expression in tumor tissue

Tumor tissues were collected 24 h after the last treatment, digested by an RNeasy mini-kit. The level of Plk1 mRNA was analyzed by RT-PCR as describe above. To determine the Plk1 expression in tumor tissue after treatments, tumor tissues were collected 24 h after the last injection. The tumor tissues were lysed and the total 80 μg protein was collected and analyzed as described above.

2.11. TUNEL assay in tumor tissue

The mice were sacrificed 16 days after the first injection, and tumor tissues were collected and fixed in 4% (w/v) paraformaldehyde. In situ TUNEL assay was performed on the excised tumor tissues using in situ cell death detection kit, POD (Roche) according to the manufacturer's protocol. Tumor sections were transferred onto the glass slide and deparaffinized. 50 μL of proteinase K (50 μg/mL) in TBS (pH 8.0) was added onto the slides and incubated for 20 min at room temperature. After rinsed with PBS for three times, the slides were incubated with TUNEL reaction mixtures for 60 min at 37 °C in a humidified atmosphere in the dark. The slides were washed with PBS. The 50 μL TUNEL reaction mixtures were mixed with 2 μL enzyme solution and 48 μL label solution. After rinsed with PBS for three times, the slides could be analyzed in a drop of PBS under CLSM by using 488 nm excitation and 530 nm emission at this state. The cells with green fluorescence were defined as apoptotic cells. DAPI was used to stain cell nucleus.

2.12. Statistical analysis

Statistical analysis was performed by using the Student's t-test with $p < 0.05$ as significant difference. The experimental results were given in the format of mean, mean ± SD in the figures.

3. Results and discussion

3.1. Synthesis siPlk1-phospholipids, preparation and characterization of siPlk1-PCNPs/DOX

The synthetic routes and chemical structures of siPlk1-phospholipids conjugates were given in Fig. 1. The 3′-thiol-modified sense and antisense siPlk1 were chosen as reactive materials, whereas the 5′-end of the antisense siRNA is essential for RNA-inducing silencing complex (RISC) loading [29]. The 3′-thiol-modified sense and antisense siPlk1 were conjugated with PDP PE via a disulfide bond, respectively, which could avoid affecting the biological activity of siPlk1. The absorbance peak at 343 nm, assigned to the released 2-pyridinethione, indicated that 3′-thiol-modified sense or antisense siPlk1 conjugated with PDP PE to form sense and antisense siPlk1-phospholipids. As shown in Fig. S1, after 2 h there is no change in the absorbance peak at 343 nm, indicating that the thiol exchange reaction was almost completed. The maximum absorbance observed was also consistent with the expected amount of 2-pyridinethione released from this reaction [30]. Subsequently, the siPlk1-phospholipids conjugate was prepared by complementary hybridization between the sense and the antisense siPlk1-phospholipid conjugates with equal amounts. Comparing with naked siRNA (MW 13,300), the siPlk1-phospholipids conjugate showed a little retarded migration in the gel, due to slight higher molecular weight of siPlk1-phospholipids (MW 15,000) (Fig. S2).

The siPlk1-PCNPs were prepared and characterized by TEM, Cryo-TEM and CLSM to prove their hypothetical structures. As shown in Fig. 2A (a and b), the TEM and Cryo-TEM images indicated that the siPlk1-PCNPs had obvious core–shell structures with three layers. Comparing with blank NPs (Fig. 2A (c)), the siPlk1-PCNPs exhibited higher electron density at the middle layer, which were speculated that the siPlk1-phospholipids conjugates were in the middle position. In comparison with siPlk1-PCNPs, siPlk1 of the siPlk1-NPs (Fig. 2 A (d)) nearly appeared in the outer layer of NPs, which suggested that the siPlk1-PCNPs had more stable and compact structures than siPlk1-NPs. To further confirm our speculation, the siPlk1-PCNPs (Fig. 2B) were formed in micrometer scales and observed under CLSM. The red fluorescence images in Fig. 2B (a) represented the DDAB and DSPE layer. Hoechst 33342 was used for staining the siRNA-phospholipids layer with blue fluorescence (Fig. 2B (b)). The overlap image in Fig. 2B (c) clearly showed that the siPlk1-phospholipids existed at the middle layer of siPlk1-PCNPs. These results indicated that the amphiphilic properties of siPlk1-phospholipids in the siPlk1-PCNPs and they can also encapsulate siPlk1 by electrostatic interaction, whereas siPlk1 in the siPlk1-NPs could only combine through electrostatic interaction, demonstrating siPlk1-PCNPs had more stable structures than siPlk1-NPs.

To evaluate siPlk1 binding abilities of the siPlk1-PCNPs and the siPlk1-NPs, gel electrophoresis and EtBr dye displacement assay were performed. The complete binding of siPlk1 in the siPlk1-PCNPs occurred at the weight ratio of NPs/siPlk1 around 24/1, leading to the absence of siPlk1 band on the agarose gel (Fig. 3A (a)) and decrease in the fluorescence of EtBr (Fig. 3B). Whereas the band of free siPlk1 of siPlk1-NPs disappeared at the weight ratio of NPs/siPlk1 around 72/1 (Fig. 3A (b)), and the fluorescence intensity decreased down to background level at the same weight ratio (Fig. 3B). Consequently, siPlk1-PCNPs with NPs/siPlk1 weight ratio of 24/1 and siPlk1-NPs with NPs/siPlk1 weight ratio of 72/1 were further used in the following investigations. Calculated from EtBr fluorescence data, siPlk1-NPs had siPlk1 loading efficiency of 1.26%, whereas siPlk1-PCNPs had 3.86%, which is three times loading efficiency compared with siPlk1-NPs, at the same quality of NPs and cationic lipids (Fig. 3C), and also higher than other reported lipid enveloped nanoparticles [31]. These results suggested that the siPlk1-phospholipids could drastically enhance the entrapment of siPlk1 in siPlk1-PCNPs, compared to siPlk1-NPs. This is likely attributed to the amphiphilic properties and negative charge with siRNA of siPlk1-phospholipids, which can self-assemble and combine to siPlk1-PCNPs with electrostatic interaction. However, free siPlk1 bound with siPlk1-NPs only through electrostatic interaction.

The size distributions and surface charge of blank NPs, siPlk1-NPs and siPlk1-PCNPs were tested by DLS assay. These results revealed that the size of blank NPs, siPlk1-NPs and siPlk1-PCNPs were 114.4, 126.1 and 139.2 nm with zeta potentials 37.0, 24.5 and 7.8 mV, respectively (Fig. S3). The data indicated that these NPs could facilitate for siPlk1 delivery to solid tumors as the enhanced permeability and retention (EPR) effect in the tumor microenvironment [32]. Meanwhile, the size distributions and zeta potentials of siPlk1-PCNPs with different NPs/siRNA ratio (w/w) were studied

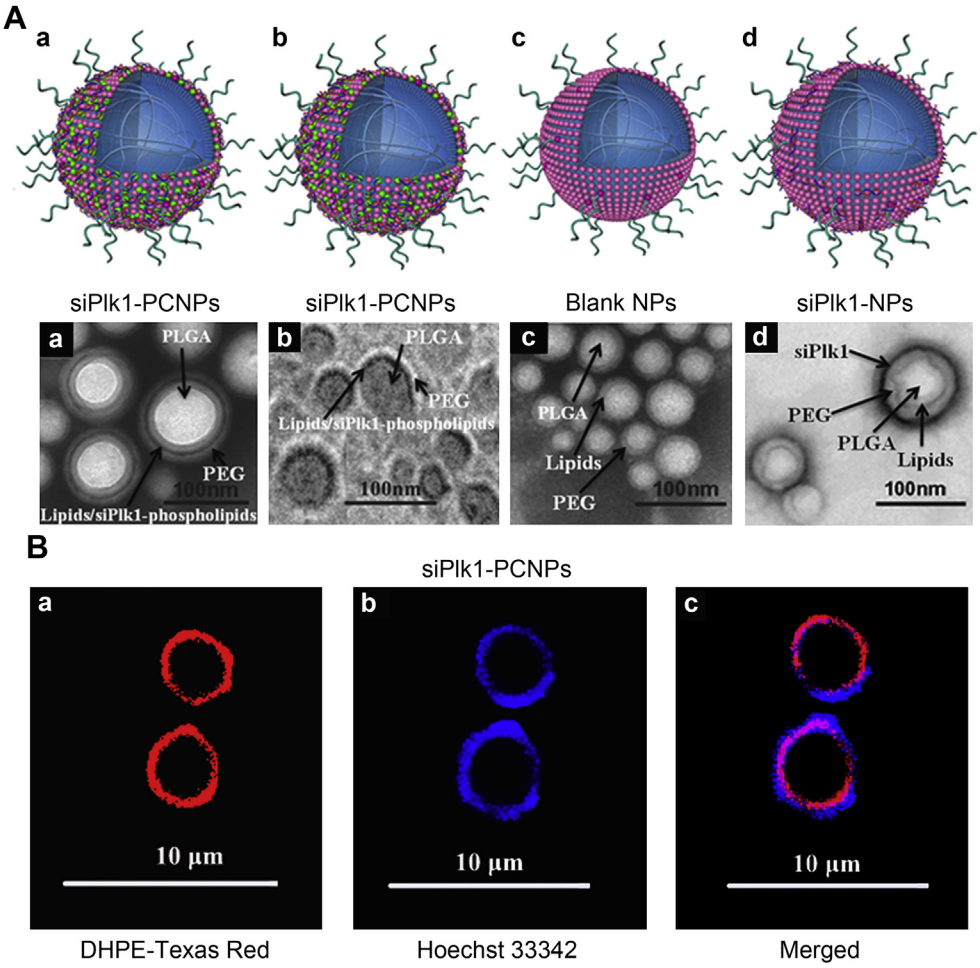

Fig. 2. A) Representative TEM and Cryo-TEM images of siPlk1-PCNPs (a and b), and TEM images of blank NPs (c) and siPlk1-NPs (d). Bar = 100 nm. B) CLSM images of the siPlk1-PCNPs taken from the DHPE-Texas Red channel (a, red), the Hoechst channel (b, blue) and the overlap of the images (c). Bar = 10 μm.

by DLS assay. With increasing the NPs/siRNA ratio (w/w) of siPlk1-PCNPs, the size of siPlk1-PCNPs decreased and the zeta potentials of siPlk1-PCNPs increased (Fig. S4). The cytotoxicity of the blank NPs was evaluated by MTT assay against *HeLa* cells. As shown in Fig. S5, the cell viability was more than 80% of survived cells when the concentration of the blank NPs was up to 1000 μg/mL and the concentration of cationic lipids DDAB was up to 93.8 μg/mL, respectively, which illustrated that the cytotoxicity of blank NPs was fairly low. Previous studies have shown that lipid and PLGA have been widely used in genes and drugs delivery, because these two materials are approved by the Food and Drug Administration (FDA) and can be accepted in clinical application [20]. Therefore, lipids and PLGA were chosen as materials for building carriers, which had potential pharmaceutical applications. The stability of siPlk1-PCNPs and siPlk1-NPs was investigated in DMEM containing 10% FBS. As shown in Fig. 3D, for 12 h incubation the size of siPlk1-PCNPs slightly increased from 138.7 to 146.7 nm. However, siPlk1-NPs presented a dramatic size increasing from 126.7 to 187.5 nm after 12 h of incubation. Thus, this result suggested that siPlk1-PCNPs had better colloidal stability in FBS compared to siPlk1-NPs, which might be due to the stable and compact structure and lower positive surface charge of the siPlk1-PCNPs. These were consistent with previous reports that the relative neutral surface charge prevented NPs from protein adsorption and aggregation [20]. This finding is important because colloidal stability in serum for any NPs determines the successful delivery of drugs to target position as it prevents particle aggregation or embolism from circulatory system and prolongs the NPs residence time in the body [33].

Under reductive condition the disulfide bonds get cleaved and release free siPlk1 from siPlk1-phospholipids conjugates. To test the release free siPlk1 from siPlk1-PCNPs, the siPlk1-PCNPs were incubated in a physiologically relevant buffer (PBS) with 10 mM dithiothreitol (DTT), which was analogous to intracellular glutathione (GSH) concentration [34]. The free siPlk1 released from siPlk1-PCNPs was tested by Quant-iT™ RiboGreen RNA Reagent and Kit. As shown in Fig. 3E, about 100% siPlk1 was released from siPlk1-PCNPs over 3 days in PBS with 10 mM DTT and about 40% siPlk1 was released from siPlk1-PCNPs at pH 7.4 in PBS for 3 days. This stability over the given time frame is very important, as the siPlk1-PCNPs could lose small amounts of the loaded siPlk1 during the system circulation prior to entering into tumor. Meanwhile, the siPlk1-PCNPs could release more siPlk1 in intracellular environment.

The siPlk1-PCNPs can encapsulate hydrophobic DOX in PLGA core. From the Fig. 3E, we found that siPlk1-phpspholipids enveloped PLGA can retard the release of DOX in PBS. About 100% DOX was released from siPlk1-NPs/DOX, but only 45% DOX was released from siPlk1-PCNPs/DOX during 9 days. This is due to the siPlk1-phospholipids provided compact and stable layer of siPlk1-PCNPs/DOX, which obviously shortening the time of release DOX than siPlk1-NPs/DOX.

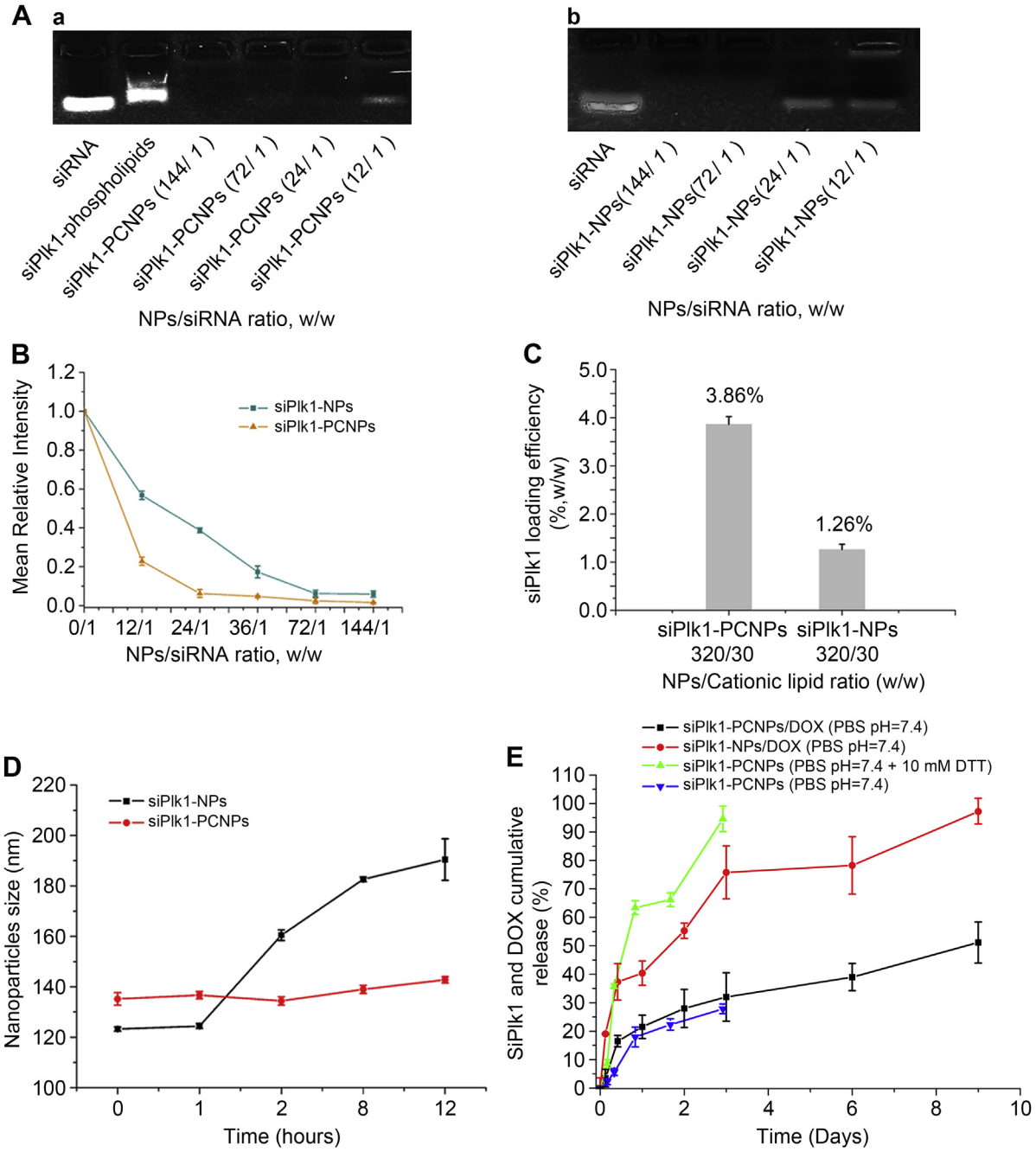

Fig. 3. A) The siPlk1 complexation capacity of the siPlk1-PCNPs (a) and the siPlk1-NPs (b) at various NPs/siRNA weight ratio determined by gel retardation assay. B) The siPlk1 complexation efficiency of the siPlk1-PCNPs and the siPlk1-NPs analyzed by EtBr dye assay. C) The siPlk1 loading efficiency of the siPlk1-PCNPs and the siPlk1-NPs with the same quality of the NPs and cationic lipids. D) Colloidal stability of siPlk1-PCNPs and siPlk1-NPs when incubated in DMEM culture medium containing 10% FBS for 12 h. The sizes were measured by DLS. E) Release profile of siPlk1 and DOX from the siPlk1-PCNPs in PBS or PBS with 10 mM DTT at 37 °C with gentle stirring. Means ± SD are shown. $n = 3$.

3.2. Gene silencing ability

We next assessed the gene silencing efficiency in *HeLa* cells. To knockdown Plk1 gene expression in the cytoplasm, NPs should efficiently get internalization into the cells and escape to cytoplasm [35,17]. Firstly, we evaluated the cell uptake as well as the intracellular fate of the siPlk1-PCNPs and siPlk1-NPs. DOX was used to track siPlk1-PCNPs and siPlk1-NPs by embedding DOX into siPlk1-PCNPs and siPlk1-NPs to form siPlk1-PCNPs/DOX and siPlk1-NPs/DOX. To explore the mechanism of siPlk1-PCNPs/DOX and siPlk1-NPs/DOX internalization, *HeLa* cells were preincubated with an endocytosis inhibitor (chlorpromazine, genistein, methyl-β-cyclodextrin (mβCD), wortmannin, or dynasore). Low temperature (4 °C) treatment was used to arrest energy-dependent endocytosis [36]. Chlorpromazine was used to inhibit clathrin-mediated endocytosis (CME), which often leads to endosomal entrapment and lysosomal degradation of DNA and siRNA, thus reducing gene transfection unless the delivery carrier is able to escape endosomes. Genistein and mβCD were used to block caveolae uptake by inhibiting tyrosine kinase and depleting cholesterol, respectively. Wortmannin is a potent inhibitor of phosphatidyl inositol-3-phosphate, which was used to prohibit macropinocytotic uptake [37]. As shown in Fig. 4A,

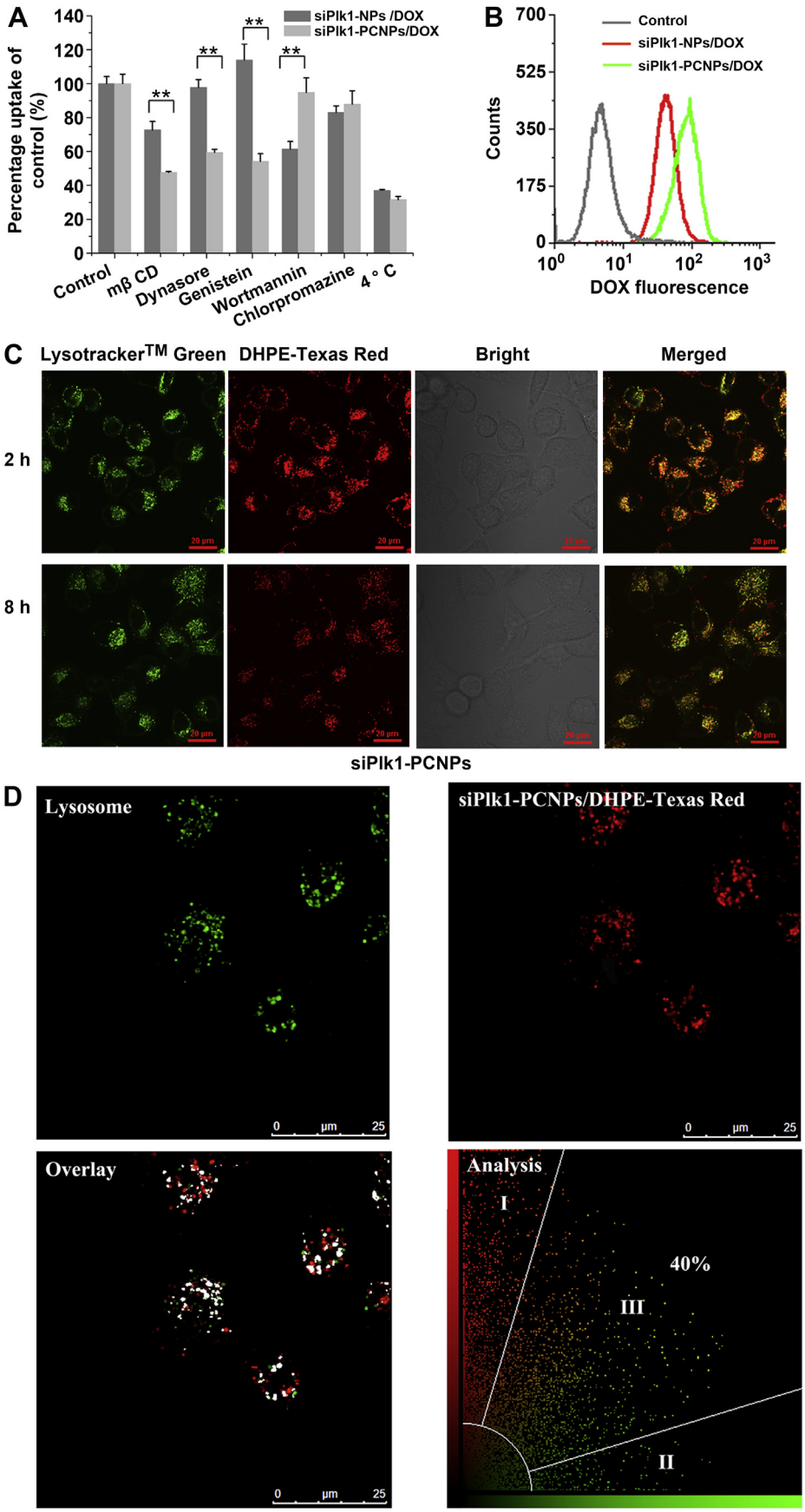

Fig. 4. The cellular uptake of siPlk1-PCNPs/DOX and siPlk1-NPs/DOX. A) Cell uptake level of siPlk1-PCNPs/DOX and siPlk1-NPs/DOX in *HeLa* cells in the presence of various endocytic inhibitors. B) Cellular uptake of siPlk1-PCNPs/DOX and siPlk1-NPs/DOX were analysized by flow cytometry after 2 h incubation. siPlk1-PCNPs/DOX and siPlk1-NPs/DOX

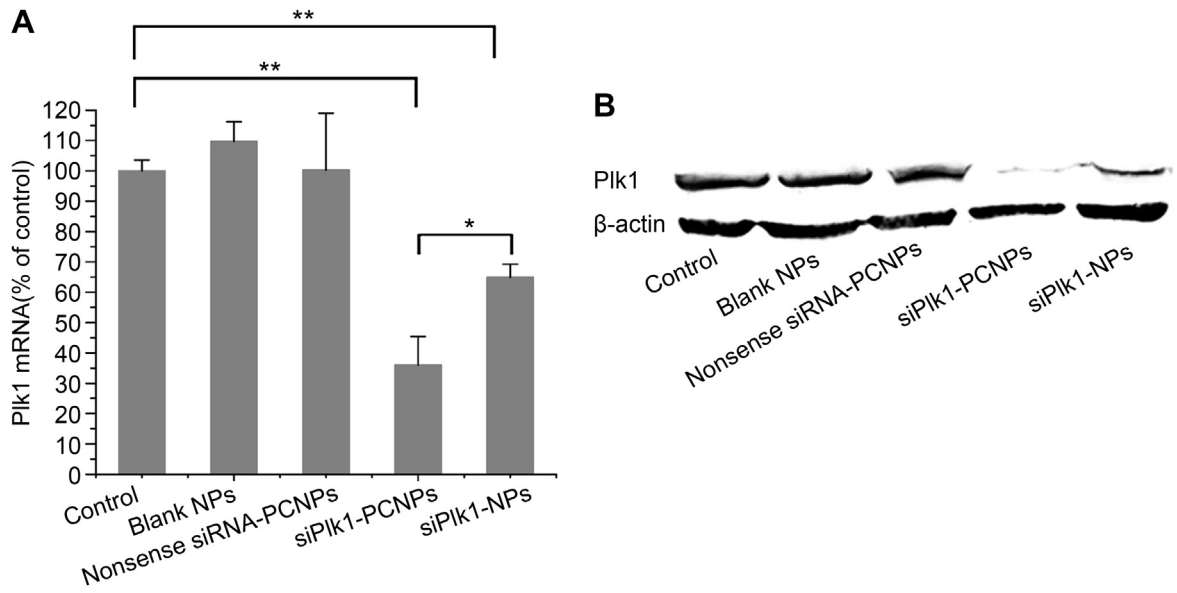

Fig. 5. A) Knockdown the expression level of Plk1 mRNA was quantified by RT-PCR. *HeLa* cells were incubated with NPs for 36 h. B) Knockdown the expression level of Plk1 protein was evaluated by Western blot analysis after incubation with *HeLa* cells for 48 h. siPlk1-PCNPs (NPs/siPlk1 (w/w) = 24/1) with a siPlk1 concentration of 200 nM and siPlk1-NPs (NPs/siPlk1 (w/w) = 72/1) with a siPlk1 concentration of 67 nM were prepared with the same weight of NPs and cationic materials. Data were presented as a mean ± SD, $n = 3$, $^{*}p < 0.05$; $^{**}p < 0.01$.

siPlk1-PCNPs/DOX and siPlk1-NPs/DOX showed different internalization mechanisms and intracellular fate. For siPlk1-NPs/DOX, the cell uptake level was inhibited by ~63% at 4 °C, suggesting that most of siPlk1-NPs/DOX were internalized via energy-dependent processes; mβCD and Chlorpromazine exerted slight inhibitory effect (~27% and 17%) while genistein, dynasore had not appreciable effect at all; ~39% inhibitory effect was observed for wortmannin, indicating that macropinocytosis was involved. Collectively, the data indicated that siPlk1-NPs/DOX entered into the cells mainly via energy-dependent endocysis and macropinocytosis. For siPlk1-PCNPs/DOX, ~68% reduction in the uptake level was observed at 4 °C. Genistein (~46%), mβCD (~52%) and dynasore (~40%) inhibited the cell uptake process. Furthermore, the cell uptake level was decreased in the presence of dynasore, which inhibited both the clathrin- and caveolar-mediated pathways by inhibiting dynamins, further demonstrating the above observed results. Only small fraction of siPlk1-NPs/DOX and siPlk1-PCNPs/DOX entered into cells via CEM. Compared with siPlk1-NPs/DOX, siPlk1-PCNPs/DOX with low charges had a slight higher rate of cell uptake (Fig. 4B). This is likely because that siPlk1-NPs/DOX and siPlk1-PCNPs/DOX had different ways to enter into the cells. The localization of NPs in cells was observed by staining endosomes and early lysosomes with Lysotracker™ Green. *HeLa* cells were incubated with siPlk1-PCNPs, which containing DHPE-Texas red for 2 h and 8 h, respectively. The CLSM analysis (Fig. 4C) showed that red spots were observed within the *HeLa* cells and siPlk1-PCNPs were mainly colocalized with the LysoTracker™ Green stained organelles after 2 h of incubation, also indicating that siPlk1-PCNPs can internalize into cells by endocytosis. Subsequently, to investigate whether siPlk1-PCNPs could efficiently escape from the endosomes/lysosome, siPlk1-PCNPs were incubated with *HeLa* cells for 8 h. As shown in Fig. 4C, the separation of the green and red fluorescence spots was more significant, suggesting that siPlk1-PCNPs could efficiently escape from the endosomes or early lysosomes to cytoplasm. The colocalization ratio of labeled endosomes/lysosome and siPlk1-PCNPs loading with DHPE-Texas Red (siPlk1-PCNPs/DHPE-Texas Red) was calculated according to equation by Leica LAS colocalization software [38].

$$\text{Colocalization ratio} = \frac{\text{Colocalization area}}{\text{siPlk1} - \text{PCNPs/DHPE} - \text{Texas red}}$$

From Fig. 4D, about 40% of siPlk1-PCNPs/DHPE-Texas red was colocalized with endosomes/lysosome, indicating that most of these NPs (about 60%) could escape from lysosome and release to the cytoplasm. Due to the conjugated phospholipids with siPlk1, there were no more places with siRNA to conjugate with fluorescent molecules. This result provided indirect proof that siPlk1 could escape from the endosomes or early lysosomes to cytoplasm. To further test whether the siPlk1 effectively escaped from endosomes or early lysosomes to knockdown the gene expression, the ability of down-regulating therapeutic target mRNA level by siPlk1 delivered by siPlk1-PCNPs and siPlk1-NPs was investigated by RT-PCR. As shown in Fig. 5A, siPlk1-PCNPs and siPlk1-NPs could significantly silence Plk1 gene expression in *HeLa* cells, leading to approximately 64% and 35.1% knockdown of Plk1 mRNA, respectively. Whereas, negative controls including treatments with PBS, blank NPs and nonsense siRNA-PCNPs showed no knockdown efficiency. Down-regulation of Plk1 mRNA expressions was subsequently accompanied by decreased Plk1 protein expression. To follow transfection abilities with siPlk1-PCNPs and siPlk1-NPs, Plk1 protein expression levels were detected by Western blot analysis. SiPlk1-PCNPs exhibited significantly enhanced silencing of Plk1 protein

contained the same concentration of DOX (2 μg/mL). C) CLSM images of endosomal escape of siPlk1-PCNPs in *HeLa* cells for 2 h and 8 h of incubation. Bar = 10 μm. D) CLSM images of lysosomes, siPlk1-PCNPs/DHPE-Texas Red, and their overlay signals after incubating siPlk1-PCNPs/DHPE-Texas Red with *HeLa* cells for 8 h. siPlk1-PCNPs was prepared with DHPE-Texas Red. Lysosomes were stained with LysoTracker™ Green. In the overlay image, the signal of siPlk1-PCNPs/DHPE-Texas Red that were colocalized with lysosome was changed to white spots by Leica LAS Co-localization software. In the analysis image, part I, II and III indicated that signals of lysosomes, siPlk1-PCNPs/DHPE-Texas Red and their colocalization spots, respectively. The colocalization ratio of lysosomes and siPlk1-PCNPs/DHPE-Texas Red were calculated by Leica LAS Co-localization software. Bar = 25 μm.

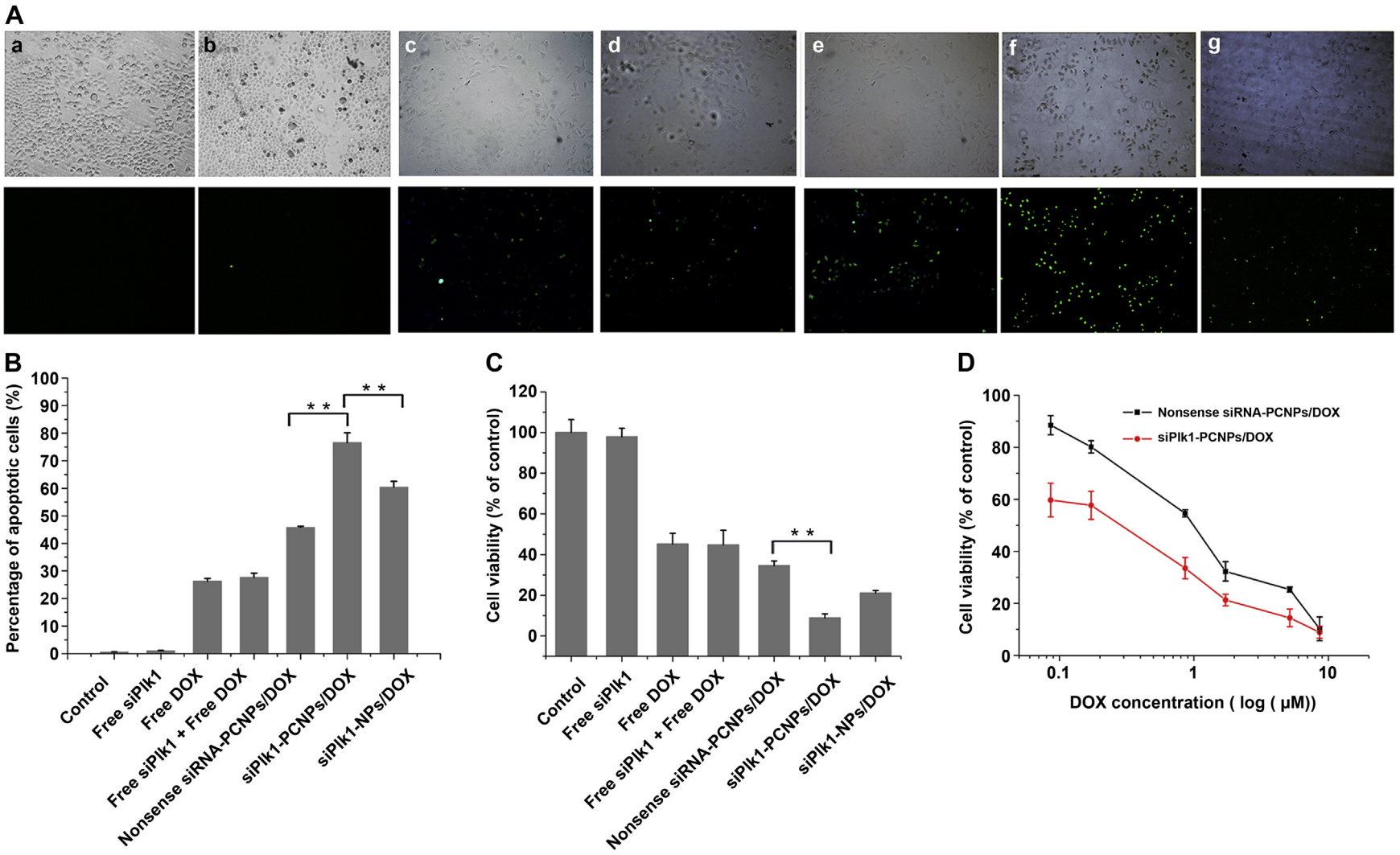

Fig. 6. A) The cell apoptosis induced by different NPs was visualized by TUNEL assay in *HeLa* cells for 72 h. The cells with green fluorescence were defined as the apoptotic cells. B) The percentage of apoptotic cells were calculated according to (A). C) The antitumor activities of free siPlk1, free DOX, free siPlk1 + free DOX, nonsense siPlk1-PCNPs/DOX, siPlk1-PCNPs/DOX and siPlk1-NPs/DOX against *HeLa* cells for 72 h. Cells were treated with various NPs at a DOX concentration of 2 μg/mL, a siRNA concentration of 200 nM for free siPlk1, free siPlk1 + free DOX, nonsense siRNA-PCNPs/DOX and siPlk1-PCNPs/DOX and 67 nM with siPlk1-NPs/DOX. D) Examination of the combined effects of siPlk1 and DOX in *HeLa* cells. siRNA concentration of 200 nM for 72 h. Data were presented as a mean ± SD, $n = 3$, $^{**}p < 0.01$.

expression compared to siPlk1-NPs (Fig. 5B). The blank NPs and nonsense siRNA-PCNPs did not knockdown Plk1 protein expression in *HeLa* cells. These results coincided with the previous data of RT-PCR that siPlk1 knockdown the gene expression in a dose-dependent manner [3].

3.3. Codelivery of siPlk1 and DOX using siPlk1-PCNPs

As shown in the previous design, the siPlk1-PCNPs can co-deliver siRNAs and hydrophobic anticancer drugs. Many studies had reported that both siPlk1 and DOX could inhibit cell proliferation through inducing cell apoptosis [18,19,39,40]. Plk1 functions in multiple steps of mitosis, and is over-expressed in *HeLa* tumor types. RNAi-mediated Plk1 depletion or inhibition of Plk1 activity with siPlk1 induced G_2/M arrest and apoptosis in *HeLa* cells. DOX (cell-cycle nonspecific antineoplastic agent) acts as cytotoxic agents inducing cancer cell apoptosis during each cycle phase. Furthermore, a Plk1 inhibitor in combination with chemotherapy (cell-cycle nonspecific antineoplastic agent) could achieve complete response and impair tumor relapse in pre-clinical studies. In this study, we hypothesized that siPlk1 and DOX co-delivery could effectively inhibit the tumor growth. Through the above RT-PCR and Western blot analysis of siPlk1-PCNPs, it was proved that siPlk1-PCNPs had highest efficiency in knocking down the Plk1 protein expression level in *HeLa* cells. Next, the combined effect of siPlk1 and DOX by siPlk1-PCNPs was examined. We characterized the physicochemical properties of siPlk1-NPs/DOX and siPlk1-PCNPs/DOX, and found that the size of siPlk1-NPs/DOX (143.7 nm) and siPlk1-PCNPs/DOX (150.3 nm) during the DOX loading process was similar to the size of siPlk1-NPs and siPlk1-PCNPs. The encapsulation efficiency of DOX in siPlk1-NPs and siPlk1-PCNPs was similar 92.4% and 93.6%, and loading efficiency of DOX was 2.4% and 2.6%, respectively.

Herein, whether the co-delivery of siPlk1 and DOX by siPlk1-PCNPs could exert the combined effect in tumor cells apoptosis and inhibit tumor cells proliferation was examined. In order to evaluate the apoptosis in *HeLa* cells, terminal deoxynucleotidyl transferase dUTP nick end labeling (TUNEL) assay was performed. The number of TUNEL-positive cells (green fluorescence) was counted to get the percentage of apoptotic cells. As shown in Fig. 6A and B, the cells incubated with PBS and naked siPlk1 exhibited very few cells apoptosis. *HeLa* cells incubated with siPlk1 and DOX-loaded various NPs showed different apoptosis levels. The siPlk1-PCNPs/DOX induced 76.4% apoptosis cells, which was much higher than that of siPlk1-NPs/DOX (60.5%), nonsense siRNA-PCNPs/DOX (45.7%) and free siPlk1 + free DOX (27.7%), indicating the combined effect of co-delivery DOX and siPlk1. These results demonstrated that siPlk1 and DOX inhibited *HeLa* cells growth through inducing the apoptosis.

MTT assay was employed to assess the antitumor activities of these NPs *in vitro*. The MTT data showed that free siPlk1 had negligible cytotoxicity against *HeLa* cells both at 72 h. Whereas, the siPlk1-PCNPs/DOX exhibited the highest cytotoxic effect among all other NPs with cell viability of 8.9% at 72 h. *HeLa* cells treated with siPlk1-NPs/DOX had 21.9% viability, nonsense siRNA-PCNPs/DOX (36.6%) and free siPlk1 + free DOX had 45.2% at 72 h (Fig. 6C). SiPlk1 was found to effectively improve the cell cytotoxicity of DOX *in vitro*, as shown by 5-fold decrease in IC50 values from the nonsense siRNA-PCNPs/DOX control (IC50 = 1.05 μM) to the siPlk1-PCNPs/DOX (IC50 = 0.21 μM) (Fig. 6D). The above results indicated that the siPlk1-PCNPs/DOX exerted the stronger combined effect than that of siPlk1-NPs/DOX, due to higher amount of siPlk1 embedded in NPs.

3.4. Tumor growth suppression in vivo

To reveal the potential of siPlk1-PCNPs/DOX as siPlk1 and DOX delivery system *in vivo*, we treated the tumor *HeLa*-bearing BALB/c nude mice with siPlk1-PCNPs/DOX. It was expected that siPlk1-PCNPs/DOX could enter into the tumor tissues by passive mechanisms, due to the nanosize of siPlk1-PCNPs/DOX. We used siPlk1-PCNPs to embed the hydrophobic DiR (absorption/emission maxima = 748/780 nm), which the high transmission of infrared light through tissues as an *in vivo* tracer in living organisms, to observe whether siPlk1-PCNPs/DOX entry into the tumor tissues by the leakiness of vessels. SiPlk1-PCNPs/DiR was injected via tail vain of mice, and was examined at 4 h after the intravenous injection by an *in vivo* imaging system. Fig. S6 showed that siPlk1-PCNPs/DiR effectively targeted in the tumor tissues for enhancing anticancer therapies. Due to DOX self-fluorescence, siPlk1-PCNPs/DOX and siPlk1-NPs/DOX were used to evaluate the tissue distribution. The tumor distributions of siPlk1-PCNPs/DOX, siPlk1-NPs/DOX and free DOX were observed 4 h after the intravenous injection in *HeLa*-bearing BALB/c nude mice. As shown in Fig. 7A, the DOX fluorescence was detected at the tumor in mice injected with siPlk1-PCNPs/DOX, siPlk1-NPs/DOX and free DOX, demonstrating the accumulation of siPlk1-PCNPs/DOX and siPlk1-NPs/DOX in tumor tissues by EPR effect. However, the strongest DOX fluorescence was observed in the tumor in case of siPlk1-PCNPs/DOX, indicating that more accumulation of siPlk1-PCNPs/DOX than siPlk1-NPs/DOX in tumor tissues. The tumor distribution of siPlk1-PCNPs/DOX, siPlk1-NPs/DOX and free DOX was also confirmed by frozen tumor tissue section observed by CLSM (Fig. S7). The *HeLa*-bearing mice injected with siPlk1-PCNPs/DOX and siPlk1-NPs/DOX had more DOX fluorescence in tumor tissues, indicating siPlk1-PCNPs/DOX and siPlk1-NPs/DOX can deliver drugs to tumors.

The tissue distribution of siPlk1-PCNPs/DOX and siPlk1-NPs/DOX was examined 24 h after the intravenous injection in ICR mice. The organs of the mice were collected and observed by an *in vivo* imaging system. A strong signal for both siPlk1-PCNPs/DOX and siPlk1-NPs/DOX was observed in the kidney, reflecting renal clearance of NPs. A higher intensity of siPlk1-NPs/DOX in the liver was observed than siPlk1-PCNPs/DOX, implicating that the liver readily captured siPlk1-NPs/DOX, which released DOX during blood circulation (Fig. 7B and C). The plasma DOX concentration was measured as a function of time post-injection. To measure the retention time of DOX in blood via NPs delivery, free DOX, siPlk1-PCNPs/DOX and siPlk1-NPs/DOX were injected to mice with the same concentration of 4 mg/kg DOX. One- and non-compartment pharmacokinetic model was used to fit the plasma concentration–time profiles (Fig. 7D). The siPlk1-PCNPs/DOX delivery extended the plasma half-time of DOX to ~10.4 h as compared with free DOX (~0.21 h). The siPlk1-NPs/DOX delivery extended the plasma half-time of DOX to ~6.6 h. Together, these findings demonstrated that siPlk1-PCNPs/DOX are able to successfully deliver DOX and siPlk1 to target tumor *in vivo* and can extensively prolong the retention time of DOX in blood. It is speculated that the low surface charge and the compact and stable structure of siPlk1-PCNPs/DOX prevented nonspecific protein adsorption and aggregation of siPlk1-PCNPs/DOX *in vivo*. Thus, more siPlk1-PCNPs/DOX accumulated in the tumor through the EPR effect and siPlk1-PCNPs/DOX had long retention time of DOX. Long-circulating siPlk1-PCNPs/DOX provided more chance for siPlk1-PCNPs/DOX accumulation in the tumor sites.

Next, we examined the antitumor growth effect of siPlk1-PCNPs/DOX after accumulation in the tumor site. Free siPlk1, free siPlk1 + free DOX, nonsense siRNA-PCNPs/DOX, siPlk1-NPs/DOX and siPlk1-PCNPs/DOX with the same concentration of siRNA 1 mg/kg and free DOX, free siPlk1 + free DOX, siPlk1-NPs/DOX, nonsense

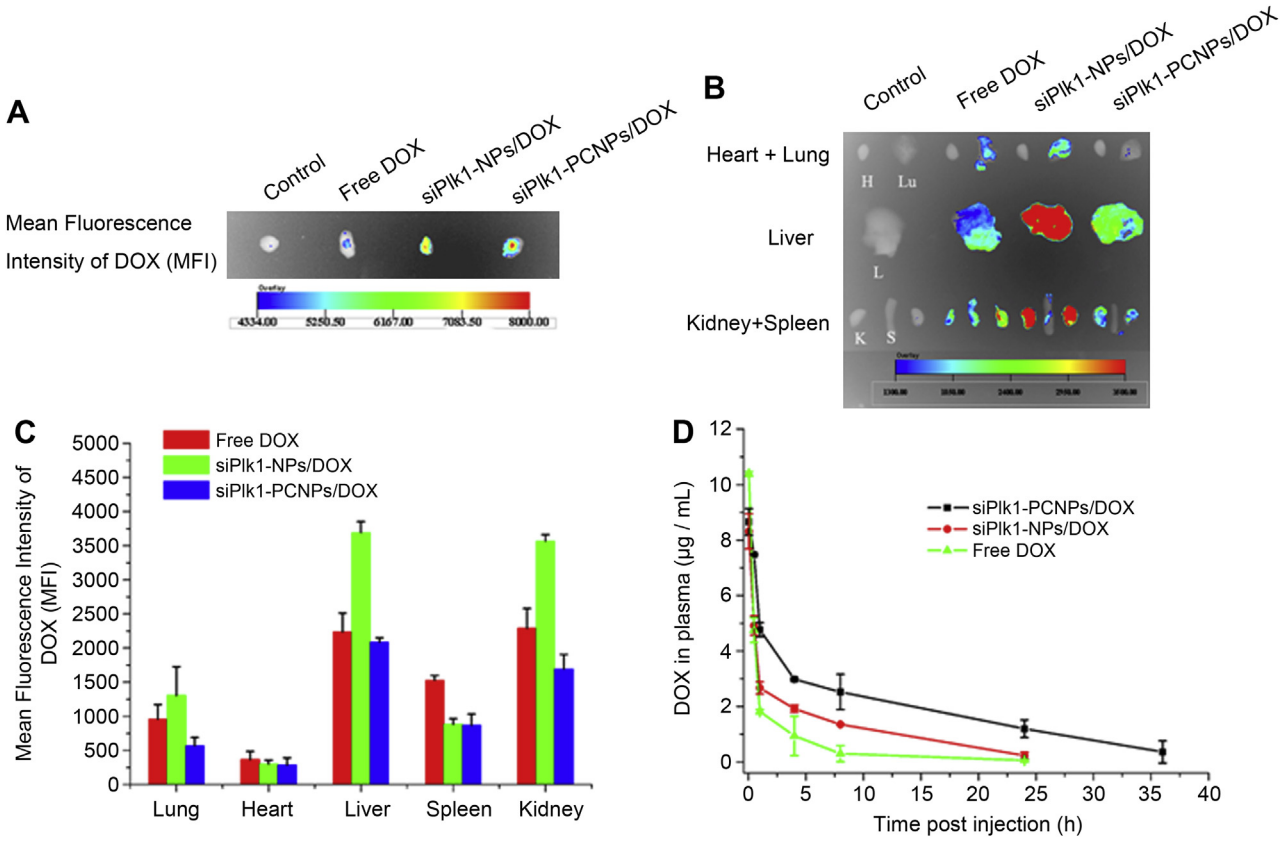

Fig. 7. *In vivo* DOX distribution in the organs after intravenous injection to mice with free DOX, siPlk1-NPs/DOX and siPlk1-PCNPs/DOX. A) Tumor distribution of DOX at 4 hour-post injection. Free DOX, siPlk1-NPs/DOX and siPlk1-PCNPs/DOX (at DOX concentration of 2 mg/kg) were intravenously injected to *HeLa*-bearing BALA/c nude mice. B) Fluorescent image of tissues distribution of free DOX, siPlk1-NPs/DOX and siPlk1-PCNPs/DOX at 1 day-post injection. Free DOX, siPlk1-NPs/DOX and siPlk1-PCNPs/DOX (at DOX concentration of 4 mg/kg) were intravenously injected to ICR mice. D) Quantitative analysis of DOX in tissue. D) Blood retention kinetics of free DOX, siPlk1-NPs/DOX and siPlk1-PCNPs/DOX in ICR mice. (at DOX concentration of 4 mg/kg) Means ± SD, $n = 4$.

siRNA-PCNPs/DOX and siPlk1-PCNPs/DOX with the same DOX dose of 2 mg/kg were intravenously injected at days 0, 2, 4 and 6. As shown in Fig. 8A, complete tumor regression was observed in siPlk1-PCNPs/DOX group, which inhibited the average tumor volume by 5.5- fold compared to the PBS control. Partial tumor regression was seen in siPlk1-NPs/DOX group, which suppressed the tumor volume by 2.3-fold, compared to the PBS control. From this result, we found that high loading efficiency of siPlk1 enhanced antitumor therapy through silencing of Plk1 gene expression. The tumor continued to grow, and no obviously inhibition of tumor growth was observed when *HeLa*-bearing mice injected free DOX, free siPlk1 and free siPlk1 + frees DOX. This is likely due to the low doses of DOX (2 mg/kg), as compared with the dose of 5 ~ 10 mg/kg as used for treatment tumors in previous reports [41,42]. After delivery into the bloodstream, the free siRNA molecules were subjected to rapid clearance from the blood through liver accumulation and renal filtration, therefore free siPlk1 did not obviously decrease the average tumor volume [43]. Moreover, compared with free DOX, nonsense siRNA-PCNPs/DOX, siPlk1-NPs/DOX and siPlk1-PCNPs/DOX had higher antitumor activity, due to nonsense siRNA-PCNPs/DOX, siPlk1-NPs/DOX and siPlk1-PCNPs/DOX delivered more DOX to tumor than free DOX, which was confirmed by distribution of DOX fluorescence in tumor tissue. Despite the low DOX dosage, siPlk1-NPs/DOX and siPlk1-PCNPs/DOX demonstrated strong antitumor activity, suggesting that the combination of DOX with siPlk1 enhanced the inhibition of tumor growth. What' more, siPlk1-PCNPs/DOX had the strongest inhibition of tumor growth, because of siPlk1-PCNPs/DOX with high siPlk1 amount, long circulating time in blood and more accumulation in the tumor. As shown in Fig. 8B, the images of tumor also confirmed that siPlk1-PCNPs/DOX displayed higher efficacy in tumor growth inhibition.

To demonstrate that inhibited tumor growth by siPlk1-PCNPs/DOX was related to Plk1 downregulation in tumor cells, the tumors were excised 24 h after the last injection. Plk1 mRNA expression was analyzed by RT-PCR. Xenografts from mice treated by siPlk1-NPs/DOX and siPlk1-PCNPs/DOX containing siPlk1 showed reduced Plk1 mRNA levels (~60% and 30% of the PBS control), respectively. Based on the RT-PCR data (Fig. 8C), *HeLa*-bearing mice injected with siPlk1-PCNPs/DOX showed the lower level of Plk1 mRNA (~30% of the PBS control) than mice injected with siPlk1-NPs/DOX (~60% of the PBS control). Meanwhile, free siPlk1, free siPlk1 + free DOX and nonsense siPlk1-PCNPs/DOX injected mice did not regulate down the Plk1 mRNA level. Tumoral Plk1 protein expression was analyzed by Western blot analyses. Western blot analyses of Plk1 protein levels in tumor tissues (Fig. 8D) revealed a significant reduction in Plk1 protein levels when the mice were treated with siPlk1-PCNPs/DOX. In contrast, there was less decrease in Plk1 protein levels after treatments with siPlk1-NPs/DOX, when compared with the treatment with the PBS. This result demonstrates that the NPs embedded lower dose of the siPlk1 had fewer effects on silencing gene expression, which coincided with the previous report that siRNA knockdown the gene expression in dose-dependent manner [3].

DOX and siPlk1 have been proved to inhibit tumor growth by inducing cell apoptosis. To examine whether cell apoptosis was induced the decrease of the tumor volume, the tumor tissues were

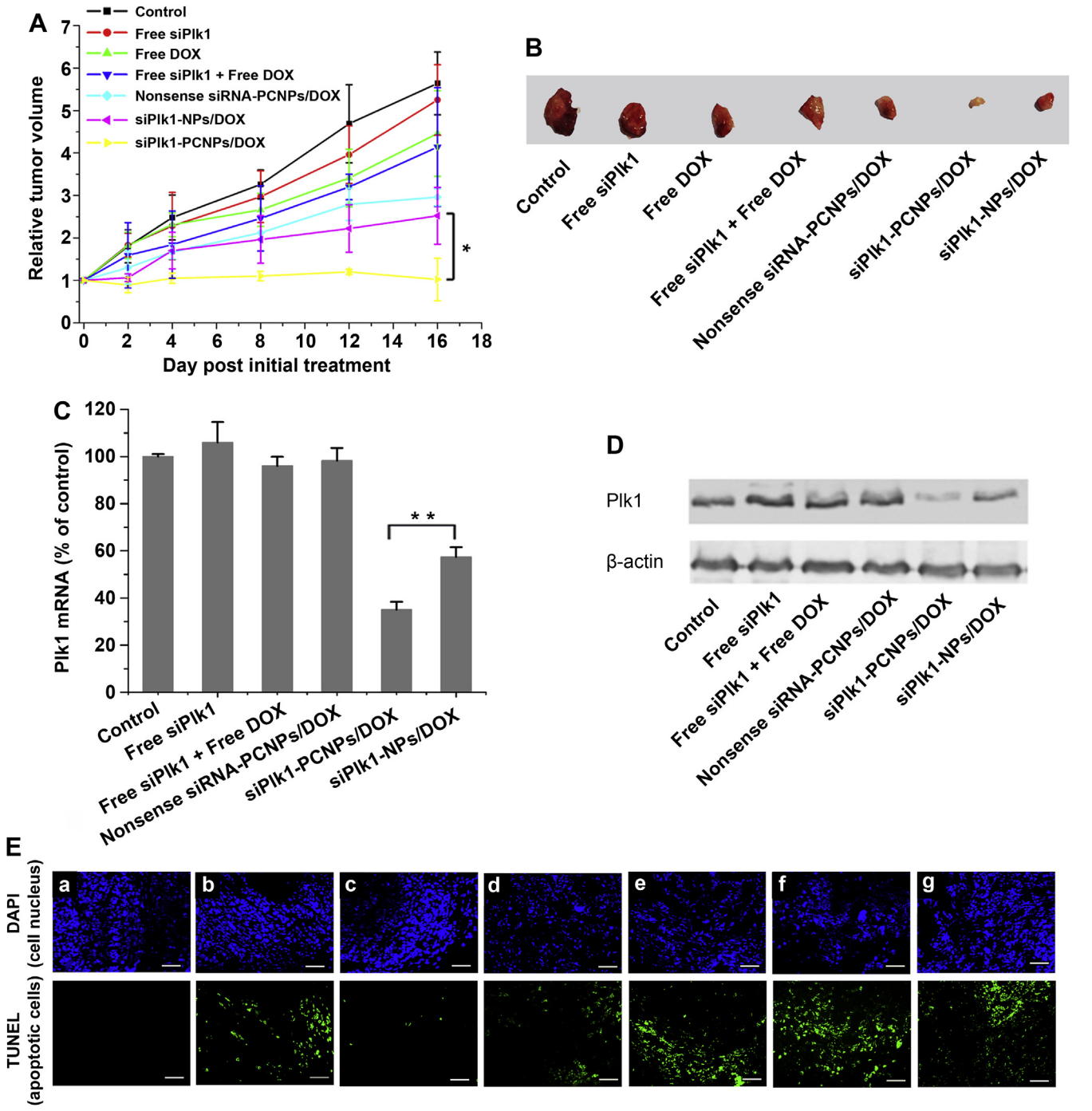

Fig. 8. A) Anticancer effects of PBS, free siPlk1, free DOX, free siPlk1 + free DOX, nonsense siRNA-PCNPs/DOX, siPlk1-PCNPs/DOX and siPlk1-NPs/DOX on *HeLa*-bearing mice. B) Picture of the tumors on day 16. C) RT-PCR analyses of Plk1 mRNA in tumor after injections of different formulations. D) Western blot analyses of Plk1 protein in tumor after injections of different formulations. The tumor tissues were collected for Western blot analyses 24 h after the last injection. Means ± SD, $n = 4$, $^{**}p < 0.01$. E) *In vivo* TUNEL analyses of tumor sections from mice receiving different formulations. In TUNEL analysis, green stains indicated apoptotic, DAPI was used to stain cell nucleus (blue). a) control, b) free DOX, c) free siPlk1, d) free siPlk1 + free DOX, e) nonsense siRNA-PCNPs/DOX, f) siPlk1-PCNPs/DOX and g) siPlk1-NPs/DOX. Bar = 50 μm.

collected for TUNEL analyses 24 h after the last injection. The combined therapy significantly increased TUNEL-positive tumoral cells, compared with free siPlk1, free DOX, free siPlk1 + free DOX and nonsense siRNA-PCNPs/DOX treatment. Notably, siPlk1-PCNPs/DOX achieved the highest cell apoptosis up to 100% and remarkably decreased the percentage of proliferating tumor cells in the studied tumor tissue section (Fig. 8E). These data indicated that siPlk1-PCNPs/DOX could enhance efficiency of treatments tumor in inducing apoptosis and prohibit the proliferation of tumor cells.

4. Conclusions

In summary, the approach of chemical conjugation of siPlk1 with phospholipids effectively increases the loading efficiency of siPlk1. With the unique properties of siPlk1-phospholipids, siPlk1-phospholipids enveloped NPs (siPlk1-PCNPs) were constructed as carriers for co-delivery of siPlk1 and DOX in *HeLa* cells or *HeLa*-bearing mice by a single-step nanoprecipitation method. Compared with siPlk1-NPs, the siPlk1-PCNPs had superior

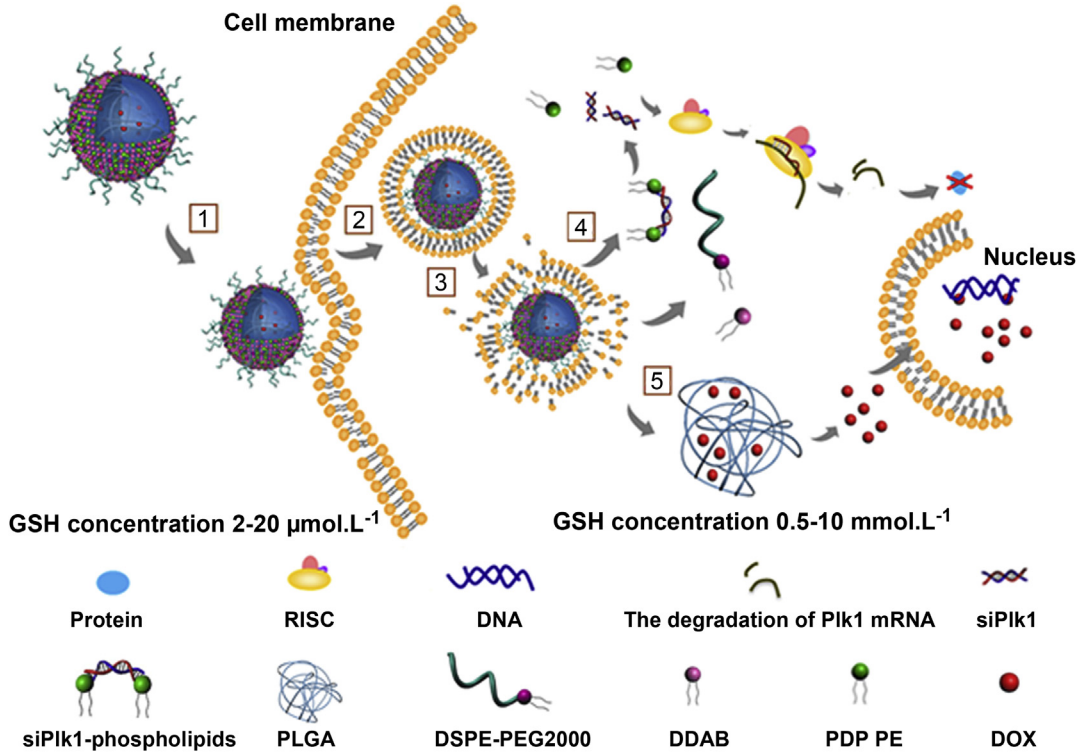

Fig. 9. Schematic illustration of siPlk1-PCNPs/DOX as co-delivery platform for siPlk1 and DOX to inhibit tumor growth in a combined way. The siPlk1-PCNPs/DOX (1) passively targeted cancerous cells through the enhanced permeability and retention (EPR) effect; (2) internalized by endocytosis; (3) escaped from endosomal/lysosomal vesicles to release the siPlk1-PCNPs; (4) released monomeric siPlk1 to down-regulate Plk1 gene expression under the high GSH concentration in the cytoplasm; (5) released the DOX entering into the nucleus to kill cancer cells with the degradation of PLGA.

characteristic siPlk1 loading capacity using less amounts of cationic materials. Meanwhile, siPlk1-PCNPs/DOX could exhibit significantly combined effect to induce tumor apoptosis and inhibit the tumor growth. The hypothetical mechanism of suppressing tumor growth by combining siPlk1 with DOX (siPlk1-PCNPs/DOX) in combined effects was shown in Fig. 9. The hybrid NPs were passively targeted to cancer cells through the EPR effect (step 1), and internalized into cells by endocytosis (step 2). After escaping from the endosomes/lysosome (step 3), the siPlk1-PCNPs entered into cytoplasm, which contained high GSH concentration. The nanoparticles released monomeric siPlk1 to down-regulate Plk1 gene expression (step 4), and finally released free DOX to enter into the nucleus with the degradation of inner core PLGA (step 5) to perform combined effects for cancer treatment. Our results suggest that the chemically conjugated siPlk1-phospholipids enveloped hybrid nanoparticles (siPlk1-PCNPs) can be potentially applied as a safe and efficient gene delivery carrier and thus an approach is constructed for enhanced gene therapy in cancer treatment.

Acknowledgements

This work was financially supported by National Natural Science Foundation of China (Grants NO. 21304099, 51203162, 51103159, 51373177), the National High Technology Research and Development Program (Grants NO. 2014AA020708, 2012AA022703, 2012AA020804), Instrument Developing Project of the Chinese Academy of Sciences (Grant No. YZ201253, YZ201313), Open Funding Project of the National Key Laboratory of Biochemical Engineering (Grant No. Y22504A169). "Strategic Priority Research Program" of the Chinese Academy of Sciences, Grant No. XDA09030301-3.

Appendix A. Supplementary data

Supplementary data related to this article can be found at http://dx.doi.org/10.1016/j.biomaterials.2014.04.033.

References

[1] Davidson BL, McCray Jr PB. Current prospects for RNA interference-based therapies. Nat Rev Genet 2011;12:329–40.
[2] Pento JT. siRNA and microRNA for the treatment of cancer. Drugs Future 2007;32:1061–6.
[3] Sun TM, Du JZ, Yao YD, Mao CQ, Dou S, Huang SY, et al. Simultaneous delivery of siRNA and paclitaxel via a "two-in-one" micelleplex promotes synergistic tumor suppression. ACS Nano 2011;5:1483–94.
[4] Xiong XB, Lavasanifar A. Traceable multifunctional micellar nanocarriers for cancer-targeted co-delivery of MDR-1 siRNA and doxorubicin. ACS Nano 2011;5:5202–13.
[5] Feng XL, Lv FT, Liu LB, Yang Q, Wang SK, Bazan GC. A highly emissive conjugated polyelectrolyte vector for gene delivery and transfection. Adv Mater 2012;24:5428–32.
[6] Nguyen DN, Green JJ, Chan JM, Langer R, Anderson DG. Polymeric materials for gene delivery and DNA vaccination. Adv Mater 2009;21:847–67.
[7] Semple SC, Akinc A, Chen JX, Sandhu AP, Mui BL, Cho CK, et al. Rational design of cationic lipids for siRNA delivery. Nat Biotechnol 2010;28:172. U18.
[8] Ewert K, Ahmad A, Evans HM, Schmidt HW, Safinya CR. Efficient synthesis and cell-transfection properties of a new multivalent cationic lipid for nonviral gene delivery. J Med Chem 2002;45:5023–9.
[9] Shu D, Shu Y, Haque F, Abdelmawla S, Guo PX. Thermodynamically stable RNA three-way junction for constructing multifunctional nanoparticles for delivery of therapeutics. Nat Nanotechnol 2011;6:658–67.
[10] Lee JB, Hong J, Bonner DK, Poon Z, Hammond PT. Self-assembled RNA interference microsponges for efficient siRNA delivery. Nat Mater 2012;11:316–22.
[11] Lee SH, Mok H, Jo S, Hong CA, Park TG. Dual gene targeted multimeric siRNA for combinatorial gene silencing. Biomaterials 2011;32:2359–68.
[12] Hong CA, Lee SH, Kim JS, Park JW, Bae KH, Mok H, et al. Gene silencing by siRNA microhydrogels via polymeric nanoscale condensation. J Am Chem Soc 2011;133:13914–7.
[13] Mok H, Lee SH, Park JW, Park TG. Multimeric small interfering ribonucleic acid for highly efficient sequence-specific gene silencing. Nat Mater 2010;9:272–8.

[14] Lee SH, Chung BH, Park TG, Nam YS, Mok H. Small-interfering RNA (siRNA)-based functional micro- and nanostructures for efficient and selective gene silencing. Acc Chem Res 2012;45:1014–25.
[15] Takemoto H, Ishii A, Miyata K, Nakanishi M, Oba M, Ishii T, et al. Polyion complex stability and gene silencing efficiency with a siRNA-grafted polymer delivery system. Biomaterials 2010;31:8097–105.
[16] Lee SJ, Huh MS, Lee SY, Min S, Lee S, Koo H, et al. Tumor-homing poly-siRNA/glycol chitosan self-cross-linked nanoparticles for systemic siRNA delivery in cancer treatment. Angew Chem 2012;51:7203–7.
[17] Takemoto H, Miyata K, Hattori S, Ishii T, Suma T, Uchida S, et al. Acidic pH-responsive siRNA conjugate for reversible carrier stability and accelerated endosomal escape with reduced IFNalpha-associated immune response. Angew Chem 2013;52:6218–21.
[18] Barr FA, Sillje HH, Nigg EA. Polo-like kinases and the orchestration of cell division. Mol Cell Biol 2004;5:429–40.
[19] Liu X, Erikson RL. Polo-like Kinase (Plk)1 depletion induces apoptosis in cancer cells. Proc Natl Acad Sci U S A 2003;100:5789–94.
[20] Zhang LF, Chan JM, Gu FX, Rhee JW, Wang AZ, Radovic-Moreno AF, et al. Self-assembled lipid-polymer hybrid nanoparticles: a robust drug delivery platform. ACS Nano 2008;2:1696–702.
[21] Shi JJ, Xiao ZY, Votruba AR, Vilos C, Farokhzad OC. Differentially charged hollow core/shell lipid-polymer-lipid hybrid nanoparticles for small interfering RNA delivery. Angew Chem 2011;50:7027–31.
[22] Lee SH, Mok H, Lee Y, Park TG. Self-assembled siRNA-PLGA conjugate micelles for gene silencing. J Control Release 2011;152:152–8.
[23] Na DH, Woo BH, Lee KC. Quantitative analysis of derivatized proteins prepared with pyridyl disulfide-containing cross-linkers by high-performance liquid chromatography. Bioconjug Chem 1999;10:306–10.
[24] Biswas S, Deshpande PP, Navarro G, Dodwadkar NS, Torchilin VP. Lipid modified triblock PAMAM-based nanocarriers for siRNA drug co-delivery. Biomaterials 2013;34:1289–301.
[25] Tang H, Yin L, Lu H, Cheng J. Water-soluble poly(L-serine)s with elongated and charged side-chains: synthesis, conformations, and cell-penetrating properties. Biomacromolecules 2012;13:2609–15.
[26] Yin LC, Song ZY, Kim KH, Zheng N, Gabrielson NP, Cheng JJ. Non-Viral gene delivery via membrane-penetrating, mannose-targeting supramolecular self-assembled nanocomplexes. Adv Mater 2013;25:3063–70.
[27] Lee SY, Kim S, Tyler JY, Park K, Cheng JX. Blood-stable, tumor-adaptable disulfide bonded mPEG-(Cys)4-PDLLA micelles for chemotherapy. Biomaterials 2013;34:552–61.
[28] Mizuno Q, Chen M, Murakami M, Kimura, et al. Accumulation of sub-100 nm polymeric micelles in poorly permeable tumours depends on size. Nat Nanotechnol 2011;6:815–23.
[29] Kanasty RL, Whitehead KA, Vegas AJ, Anderson DG. Action and reaction: the biological response to siRNA and its delivery vehicles. Mol Ther 2012;20:513–24.
[30] Ghosh S, Basu S, Thayumanavan S. Simultaneous and reversible functionalization of copolymers for biological applications. Macromolecules 2006;39:5595–7.
[31] Taratula O, Kuzmov A, Shah M, Garbuzenko OB, Minko T. Nanostructured lipid carriers as multifunctional nanomedicine platform for pulmonary co-delivery of anticancer drugs and siRNA. J Control Release 2013;171:349–57.
[32] Stylianopoulos T. EPR-effect: utilizing size-dependent nanoparticle delivery to solid tumors. Ther Deliv 2013;4:421–3.
[33] Dobson J. Gene therapy progress and prospects: magnetic nanoparticle-based gene delivery. Gene Ther 2006;13:283–7.
[34] Wang W, Ballatori N. Endogenous glutathione conjugates: occurrence and biological functions. Pharmacol Rev 1998;50:335–56.
[35] Troiber C, Wagner E. Nucleic acid carriers based on precise polymer conjugates. Bioconjug Chem 2011;22:1737–52.
[36] Gabrielson NP, Lu H, Yin LC, Kim KH, Cheng JJ. A cell-penetrating helical polymer for siRNA delivery to mammalian cells. Mol Ther 2012;20:1599–609.
[37] Khalil IA, Kogure K, Akita H, Harashima H. Uptake pathways and subsequent intracellular trafficking in nonviral gene delivery. Pharmacol Rev 2006;58:32–45.
[38] Wei W, Lv PP, Chen XM, Yue ZG, Fu Q, Liu SY, et al. Codelivery of mTERT siRNA and paclitaxel by chitosan-based nanoparticles promoted synergistic tumor suppression. Biomaterials 2013;34:3912–23.
[39] Neville-Webbe HL, Evans A, Coleman RE, Holen I. Presence of BRCA1 gene enhances levels of apoptosis induced by combination treatment with doxorubicin (DOX) and zoledronic acid (ZOL). Breast Cancer Res Treat 2004;88:73.
[40] Strebhardt K. Multifaceted polo-like kinases: drug targets and antitargets for cancer therapy. Nat Rev Drug Discov 2010;9:643. U24.
[41] Gou PF, Liu WW, Mao WW, Tang JB, Shen YQ, Sui MH. Self-assembling doxorubicin prodrug forming nanoparticles for cancer chemotherapy: synthesis and anticancer study *in vitro* and *in vivo*. J Mater Chem B 2013;1:284–92.
[42] Taniguchi Y, Kawano K, Minowa T, Sugino T, Shimojo Y, Maitani Y. Enhanced antitumor efficacy of folate-linked liposomal doxorubicin with TGF-beta type I receptor inhibitor. Cancer Sci 2010;101:2207–13.
[43] Huang YY, Hong JM, Zheng SQ, Ding Y, Guo ST, Zhang HY, et al. Elimination pathways of systemically delivered siRNA. Mol Ther 2011;19:381–5.